



Ozone trends and drivers at a Southern Hemisphere background site in Chile

Laura Gallardo^{1,2}, Charlie Opazo^{1,2}, Camilo Menares^{1,2}, Kevin Basoa^{1,3}, Nikos Daskalakis⁴, Maria Kanakidou^{4,5,6}, Carmen Vega⁷, Nicolás Huneeus^{1,2}, Roberto Rondanelli^{1,2} and Rodrigo Seguel^{1,2}

- ¹ Center for Climate and Resilience Research (CR2, FONDAP 15110009), Santiago, Chile
- ² Departamento de Geofísica, Facultad de Ciencias Físicas y Matemáticas, Universidad de Chile, Santiago, Chile
- ³ Ministry of the Environment, Chile
- ⁴ Laboratory for Modeling and Observation of the Earth System (LAMOS), Institute of Environmental Physics (IUP), University of Bremen, Bremen, Germany
 - ⁵ Environmental Chemical Processes Laboratory, Department of Chemistry, University of Crete, Heraklion, Greece
 - ⁶ Center for the Study of Air Quality and Climate Change, Foundation for Research and Technology Hellas, Patras, Greece
 - ⁷ Dirección Meteorológica de Chile
- Correspondence to: Laura Gallardo (lgallard@u.uchile.cl)

Abstract

Tropospheric ozone (O₃) is a significant anthropogenic climate forcer with uncertain distribution in the Southern Hemisphere due to sparse observations. This study analyzes 28 years of in situ ozone, methane, carbon monoxide, and meteorological data at Tololo (30.17° S, 70.80° W, 2154 m a.s.l.), Chile, integrating reanalysis and atmospheric chemistry modeling. Here we identify a rising ozone trend of 2.1±0.8 ppbv per decade since 2006, primarily driven by increasing background methane. We quantify contributions from biomass burning and stratosphere-to-troposphere transport, each adding approximately 5 ppbv per event during late winter and spring O₃ maximum. Stratospheric intrusions are linked to synoptic-scale troughs and cutoff lows, modulated by El Niño Southern Oscillation phases. These findings enhance understanding of ozone variability in the Southern Hemisphere free troposphere and underscore the importance of sustained observations at Tololo to monitor tropospheric ozone dynamics amid climate change.

1. Introduction

Tropospheric ozone (O₃) is the third largest anthropogenic climate forcer (Checa-Garcia et al., 2018; Forster et al., 2021; Myhre et al., 2013; Skeie et al., 2020). It also affects the terrestrial carbon sink by altering photosynthesis (Fu et al., 2020; Kumar Mishra et al., 2024). Further, it is central to the cleansing capacity of the atmosphere as it is an oxidant and the precursor of the hydroxyl radical (OH) (Murray et al., 2014; Thompson, 1992), which in turn determines the lifetime of the second largest anthropogenic climate forcer, i.e., methane (He et al., 2020; Young et al., 2013). Also, tropospheric ozone adversely affects human health (Fleming et al., 2018; Nuvolone et al., 2018) and vegetation (Ainsworth, 2017; Mills et al.,





2016). On the other hand, oxidants, including O₃, mediate the formation of secondary particles that are key to air quality and radiative balance, particularly at the regional scale (Karset et al., 2018; Turnock et al., 2020).

In the remote troposphere, ozone (O₃) is primarily produced through the oxidation of long-lived species such as methane (CH₄), carbon monoxide (CO), and secondary oxygenated compounds, provided that sufficient nitrogen oxides (NOx = NO + NO2) are present (Crutzen, 1988; Crutzen et al., 1999). In contrast, in more polluted regions, O₃ formation is dominated by the oxidation of short-lived volatile organic compounds (VOCs) (Archibald et al., 2020; Monks et al., 2015). In the absence of nitrogen oxides, different oxidation pathways are favored that lead to the destruction of ozone. The second largest contribution to the tropospheric ozone budget is stratosphere-to-troposphere transport (STT) (Archibald et al., 2020; Young et al., 2018). Near the surface, O₃ is removed from the atmosphere by dry deposition (Clifton et al., 2020). All these processes, and particularly photochemical production and destruction, result in a highly non-linear behavior that is sensitive to changes in precursors VOCs and nitrogen oxides— and climate variability and change (Barnes et al., 2016; Griffiths et al., 2021; Inness et al., 2015).

According to the sixth assessment report (AR6) of the Intergovernmental Panel on Climate Change (IPCC), tropospheric ozone has exhibited increasing trends since the mid-1990s, with rates of 1 to 4 ppbv/decade in the Northern Hemisphere (NH), 1 to 5 ppbv/decade in the tropics, and less than 1 ppbv/decade in the Southern Hemisphere (SH) (Gulev et al., 2023). These trends are influenced by changes in ozone precursors—whose interactions are highly nonlinear—and by transport processes, particularly variations in stratosphere-troposphere exchange (STE)(Li et al., 2024; Škerlak et al., 2014). Global warming is projected to widen the Hadley circulation, thereby altering the location and intensity of STE (Hu et al., 2018; Lu et al., 2019). Additionally, meteorological phenomena such as the El Niño Southern Oscillation (ENSO), Quasi-Biennial Oscillation (QBO), and Madden-Julian Oscillation (MJO) also modulate tropospheric ozone levels (e.g., Sekiya and Sudo, 2012).

Observations from various platforms—including aircraft, ozone sondes, and satellites—indicate that the global burden of tropospheric O₃ has increased since the second half of the 20th century (Gaudel et al., 2018). Until the 1980s, high ozone concentrations were observed over and downwind of North America and Europe, regions where anthropogenic emissions of O₃ precursors were at their peak. Since then, these emissions have shifted toward lower latitudes, resulting in elevated O₃ levels in East and South Asia (Szopa et al, 2021). Global-scale atmospheric chemistry modeling studies attribute the rise in tropospheric O₃ since pre-industrial times primarily to increasing anthropogenic emissions of O₃ precursors (e.g., Griffiths et al., 2021; Szopa, 2021). This increase has contributed to a global climate forcing of 0.47±0.23 W/m², as reported in AR6 (Forster et al, 2021). Because the lifetime of tropospheric O₃ is relatively short (25.5 ± 2.2 days on average) (Griffiths et al., 2021), its distribution is spatially heterogeneous, reflecting the complex, nonlinear interactions among precursors and atmospheric dynamics. The approximately 50% uncertainty in the estimate of global climate forcing from tropospheric O₃ arises from two main sources: first, the lack of pre-industrial ozone observations, and second, uncertainties in the current distribution of tropospheric O₃ (Szopa, 2021 and references therein). Recent advances using oxygen isotopic studies (e.g., clumped isotopes, ¹⁸O)80) have helped constrain the former, suggesting a less than 40% increase in tropospheric O₃ burden

Equator (Hoesly et al., 2018; Szopa et al, 2021).





from preindustrial times to 2005, with most of this increase occurring between 1950 and 1980 in the Northern Hemisphere.

(Yeung et al., 2019). The latter source of uncertainty is due to the scarcity and uneven spatial coverage of observations, especially in the upper troposphere of the tropics and subtropics, where ozone's radiative forcing is most effective (Kuai et al., 2017). Global anthropogenic emissions of CO and NOx, mainly from fossil fuel combustion, rose sharply between 1950 and 1980, followed by a period of slower growth (NOx) or decline (CO), with a noticeable shift in emission hotspots toward the

Methane (CH₄) is a major contributor to increased ozone in the background atmosphere. Globally averaged in situ observations indicate that CH₄ concentrations have risen from approximately 1630 ppbv in early 1984 to 1943 ppbv in late 2024 (https://www.gml.noaa.gov/ccgg/trends_ch4/, retrieved Feb 2 2025). This increase has not been uniform: there was a sharp rise between 1980 and 1990, a plateau from 1990 to the mid-2000s, and then another sharp increase to the present, largely driven by anthropogenic activities (Gulev et al., 2023). According to Zhang et al. (2021), methane accounted for about 27% of the total increase in the ozone burden between 1980 and 2010. Due to its relatively long atmospheric lifetime (about 9 years), methane influences global tropospheric O₃ levels regardless of its emission source region. In contrast, changes in CO, VOCs, and NOx—each with much shorter atmospheric lifetimes—result in more localized and regionally differentiated impacts on ozone. Modeling studies indicate that the tropospheric O₃ burden is particularly sensitive to changes in precursor emissions in tropical and subtropical regions, which have also experienced rapid increases in tropospheric O₃, especially in Southeast Asia (Zhang et al., 2016, 2021).

Biomass burning is a significant source of O₃ precursors, including remote areas in the SH as inferred from both modeling and observational studies (Bourgeois et al., 2021; Daskalakis et al., 2022). This source is particularly relevant in the SH extratropics during the austral spring, where long-range transport of fire emissions from Southeast Asia, South America, Southern Africa, and Oceania, affects the tropospheric O₃ column over the otherwise pristine Southeastern Pacific (Daskalakis et al., 2022). Bourgeois et al. (2021) estimate the contribution of biomass burning to tropospheric O₃ to be 2 to 10 times larger than that of urban (fossil fuel burning) in the SH, a contribution that is typically underestimated by global chemistry transport models.

Cooper et al. (2020) reported surface O₃ trends at 27 globally distributed remote locations, of which only 7 were in the SH. This study provided, *i.a.*, a range of regional long-term (at least 20 years) O₃ trends for the evaluation of global chemistry-climate models. In the SH, most stations (5 out of 7) showed positive trends, while in the NH it was evenly split between positive and negative trends. A similar result is found by Christiansen et al. (2022), who considered 13 surface stations in the SH. Christiansen et al. (2022) also reports that models do not capture long-term O₃ trends throughout the troposphere around the world, typically underestimating those trends (They considered 25 ozone sounding sites over the period 1990-2017).

In summary, observations of ozone in remote regions—especially in the tropics and subtropics—are essential for quantifying its variability and trends, validating atmospheric chemistry models, and accurately estimating the climate forcing associated with tropospheric ozone. However, measurements in the subtropical Southern Hemisphere mid-troposphere remain





scarce, limiting our understanding of ozone drivers in this region. In this study, we combine 28 years of in situ measurements of O3 and meteorological variables at Tololo (30.17° S, 70.80° W, 2154 m a.s.l., Chile) with reanalysis data and measurements of CO and CH₄ to assess changes in the O₃ trend. Furthermore, by employing a Generalized Additive Model (GAM) and three-dimensional atmospheric chemistry simulations, we evaluate the role of background CH₄ and other factors in explaining the observed increase in O₃, as well as the contributions of biomass burning and stratosphere-to-troposphere transport, particularly during the late winter and spring ozone maximum.

The paper is organized as follows. In section 2 we describe the observation site in some detail as well as the data used in our study. Also, we describe the application of a Generalized Additive Model (GAM) to assert the dependence of the ozone time series on methane, local and remote meteorology, seasonality, etc. Results and discussion are presented in section 3. Section 4 provides a summary and conclusions of this work.

2. Data and methodology

2.1 Site description

The Chilean Meteorological Service (In Spanish, *Dirección Meteorológica de Chile*, DMC), under the auspices of the Global Atmospheric Watch Programme (GAW) of the World Meteorological Organization (WMO), has maintained the Tololo station (30.17° S, 70.80° W, 2154 m a.s.l.) in the premises of the Interamerican Southern Astronomical Observatory since late 1995. The site is located about 50 km east of the Chilean coast, where the fast-growing conurbation of La Serena-Coquimbo is located. Despite this urban expansion, there is no evidence of increased impact from local emissions at Tololo, as discussed in later sections. Details on urban population and infrastructure in the region are provided in Figure S1 of the Supplementary Material.

In addition to the urban areas in the surroundings of Tololo, there is a potential influence of the large urban areas to the south of it: Santiago, the capital city, and the conurbation of Valparaíso-Viña del Mar (Anet et al., 2017) as illustrated in Figure 1. In this case we consider whole provinces as there are smaller urban areas functionally connected to Santiago and Valparaíso-Viña del Mar cities. While in 1992 the population of Santiago (Valparaíso-Viña del Mar) was 5258 k inhabitants (808 k inhabitants), in 2024 it is estimated to be 8421 k inhabitants (1104 k inhabitants), corresponding to a 60% (37%) percentage growth rate. We show evidence that this influence is sporadic.



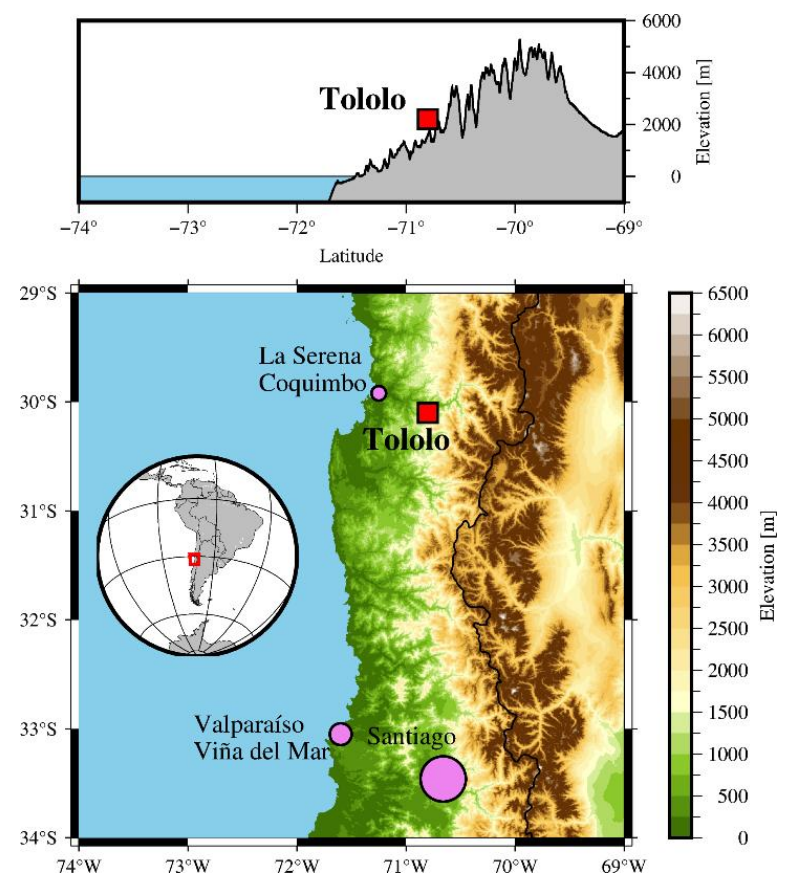


Figure 1. Location of Tololo station. The upper map shows Tololo's location in the west of South America. The upper map also shows Tololo's position on a mountain top above 2000 m a.s.l along a transect at 30°S. The lower map shows the complex topography of the area with the Andes cordillera a few kilometers east of the Tololo site. The location of three major urban areas, i.e., the conurbations of La Serena-Coquimbo, Valparaíso-Viña del Mar and the capital city of Santiago are also shown.

Over the years, this station's topography and atmospheric circulation have been described in some detail (Anet et al., 2017; Gallardo et al., 2000; Kalthoff et al., 2002; Rondanelli et al., 2002). The area surrounding Tololo is characterized by highly complex topography, with deep valleys and the Andes cordillera located just 30 km east of Cerro Tololo, reaching elevations up to 6 km a.s.l. Most of the time, Tololo is immersed in the free troposphere and influenced by the subsidence regime of the South Pacific high, which brings clear sky conditions—a factor that has contributed to the establishment of numerous astronomical observatories in the region. In winter, the subtropical jet stream (STJ) is located on average at 30°S. From time to time, cutoff lows and deep troughs from higher latitudes may reach the Tololo area inducing tropopause breaks and/or upward mixing of marine boundary layer air. Above 4 km a.s.l., large-scale westerly winds prevail, while northerly winds are observed in a band between 2 and 4 km a.s.l., which results from the blocking effect of the westerly flow by the Andes. In addition to these features, a radiatively driven circulation that is intensified in summer is present with up-slope (down-slope) winds during the afternoon (night/early morning) at Tololo.





2.2 In situ measurements at Tololo

Surface O₃ has been measured in Tololo since November 1995. The technique used is UV absorption as detailed in Anet et al. (2017). This station is part of GAW, and data used here (hourly averages between November 1995 and December 2023) were downloaded from the EBAS database (https://ebas.nilu.no/, latest access: 1 August 2024), thus it is subject to quality standards and rigorous scrutiny.

The station was equipped with a new ozone monitor and a CO, CO₂, and CH₄ analyzer (Picarro Inc. G2401) by the Swiss Federal Laboratories for Materials Science and Technology (EMPA) in 2013. CO data are available until 2022 and CH₄ until 2023. Data were downloaded from https://gaw.kishou.go.jp/, latest access: 1 August 2024. Calibration procedures are detailed in the metadata.

Standard meteorological data –wind, temperature, pressure and solar radiation– are also measured at the station. The data for the period between 1995 and 2023 were retrieved from the data base of the Chilean Weather Service (https://climatologia.meteochile.gob.cl/application/informacion/fichaDeEstacion/300034, last access: 1 October 2024). As explained later, these data were used to correct the reanalysis data at 775 hPa. We did not use the observed data because there were significant data gaps, particularly regarding humidity.

2.3 Reanalysis and large-scale variability data

We used ERA5 data (Hersbach et al., 2020) instead of the local time series for temperature, humidity, and winds, extracting values at 30.25°S, 70.75°W and 775 hPa, the grid point closest to Tololo's actual location. A bias was identified in the ERA5 time series when compared to available in situ measurements (see Figure S2). To correct for this, we applied a Quantile Delta Mapping bias correction to the ERA5 data for Tololo. The correction was performed separately for each month and hour: for example, to adjust values at 00:00 in January, all observational and ERA5 data for January at that hour, as well as data from two hours before and after (a 5-hour window), were used to calculate the adjustment, which was then applied to the January 00:00 data. This procedure was repeated for each hour and month, resulting in a specific correction for every month-hour combination.

We also used ERA5 data to identify stratospheric intrusions. To this end, we utilized geopotential height and vertical velocity at 500 hPa to estimate horizontal anomaly composites, as well as potential vorticity and specific humidity between 900 and 200 hPa to estimate a vertical cross section (longitude-pressure) along 30.25°S. To calculate anomalies, firstly we estimated the climatological annual cycle between 1995-2023 based on daily data. Thereafter we applied a Fourier filter to eliminate high frequency fluctuations (sub seasonal). Then, we calculated the anomaly as the difference between the 24-hour running mean of the time series and the smoothed climatology.

To assess how climate variability affects long-term trends at Tololo, we considered ENSO, QBO and MJO in our GAM analysis described later. For El Niño-La Niña we used the Multivariate ENSO Index version 2 (MEI). It corresponds to the bi-monthly mean of the principal component of the combined empirical orthogonal function of five observed variables





over the tropical Pacific: sea level pressure, surface temperature, surface zonal wind, surface meridional wind, and outgoing longwave radiation. This index is elaborated by NOAA Physical Sciences Laboratory (https://www.psl.noaa.gov/enso/mei, last access: 30 March 2024).

For QBO, we used the monthly mean zonal wind measured by meteorological soundings in Singapore (01.22N, 103.55E) in 50 (QBO50) and 30 (QBO30) hPa. Monthly means are calculated from daily data in Singapore. Data were obtained from the National Aeronautics and Space Administration (NASA), at the Goddard Space Flight Center (GSFC) (https://acdext.gsfc.nasa.gov/Data services/met/qbo/QBO Singapore Uvals GSFC.txt, last access: 25 October 2024).

In the case of MJO, we used the Real-Time Multivariate (RMM) MJO daily index (Gottschalck et al., 2010; Wheeler & Hendon, 2004). It corresponds to the first two principal components of the combined empirical orthogonal functions between 15°N-15°S of anomalous 200 and 850-hPa zonal winds and outgoing longwave radiation. It was retrieved from the Bureau of Meteorology Australia (http://www.bom.gov.au/climate/mjo/, last access: 29 May 2024).

2.4 Other ancillary data

As indicated before, CH₄ has been recorded at Tololo for the period 2013-2023. To complete the time series to the period before 2013, we used data collected at Rapa Nui (Easter Island, 27.8S, 109.8W, 51m a.s.l.), which is an ozone sounding monitoring station under GAW (Gallardo et al., 2016). In addition to ozone soundings, the National Oceanic and Atmospheric Administration (NOAA, https://gml.noaa.gov/dv/site/?stacode=EIC) maintained, *i.a.*, weekly CH₄ flask measurements on the island between 1994 and 2019. Firstly, we compared both time series over the period 2013-2019, and we found slightly higher values at Tololo (See methane at Rapa Nui and Tololo in Figure S 3). As the differences in methane between both sites were deemed minor – possibly due to oceanic upwelling near Tololo (Weber et al., 2019)—and given the long turn-over time of CH₄, we decided to extend Rapa Nui CH₄ by means of a simple linear regression of simultaneous measurements. We took Tololo measurements at 22 UTC on the same days as they are available at Rapa Nui. Once the regression had been performed, we used it to extend the CH₄ time series for Rapa Nui until 2023 and used them for Tololo. These data were then used in our GAM to assess the influence of methane on the long-term trend of ozone measured at Tololo. Lastly, we estimated a smooth time series (with annual seasonality) and a smooth trend (without seasonality) to represent the new time series for CH₄ according to (Thoning et al., 1989). We used the code available at NOAA (https://gml.noaa.gov/aftp/user/thoning/ccgcrv/, last access 15 October 2024).

2.5 Identifying the influence of biomass burning

We use outputs from a global atmospheric chemistry model to estimate the contribution of biomass burning at Tololo. The model is TM4-ECPL as described in Daskalakis et al. (2022). The model has a horizontal resolution of 3° longitude×2° latitude, with 34 hybrid vertical layers up to 10 hPa. The model was run over the period 1995 and 2015. Differently from Daskalakis et al. (2022) the model has been re-run using updated emissions as used in AR6, i.e., emissions as described in





Hoesly et al. (2018) and Van Marle et al. (2017). The model was run with and without biomass burning to estimate the contribution of this source of precursors to ozone.

Despite its resolution, the model captures the seasonal and, partly the day-to-day, possibly synoptical in origin, variability as inferred from the comparison with daily mean observations of CO. However, there is a positive model bias (~7 ppbv), and a larger distance between model and observations of CO in the upper tail of the data distribution (See Figure S 4). Hence, we performed a bias correction of the model data. To do so, we followed a similar approach to that used for ERA 5 data, and as also applied by Staehle et al. (2024) and implemented by Schwertfeger et al. (2023). Thereafter, we applied the bias correction to the rest of the model data set. We assumed that the adjusted model CO kept the same ratio with biomass burning CO as the original data, which allowed us to also adjust the biomass signal. The characterization regarding the influence of biomass burning is restricted to the period between 1995 and 2015 for which we have TM4-ECPL data.

2.6 Identifying stratospheric intrusions

Stratospheric intrusions are characterized by relatively high O₃ and low water vapor mixing ratios, thus we used the hourly time series of O₃ and specific humidity at Tololo to identify stratospheric intrusions. Firstly, we calculated enhancements of O₃ over a 10-day running mean of O₃ and a simultaneous reduction in specific humidity over a 10-day period similarly to Cui et al. (2009). Differently from Cui et al. (2009), we also averaged specific humidity and did not use relative humidity but specific humidity. After a careful visual inspection of the data, we defined a stratospheric intrusion event as a continuous period where simultaneously hourly O₃ was 10% above the 10-day running average, and hourly specific humidity was less than 70% of the 10-day running mean. The minimum duration of an event was set to be 12 hours or half a day to account for fast passing synoptic and sub synoptic perturbations. To avoid identification problems due to missing data, high frequency variability or errors associated with using specific humidity from ERA5, we slightly relaxed the continuity criterion. We allowed up to a maximum of 6 hours after the event in which the above criteria might not be met in all hours and still be considered part of the same event. While many criteria may be established to quantify the intensity of an event, we opted to consider the duration of the event as the intensity indicator. Also, TM4-ECPL has a dedicated stratospheric ozone tracer that was used to estimate the ozone of stratospheric origin arriving in Tololo. We compared the results from the empirical method indicated above with the model outputs.

2.7 Estimating trends

The term trend is not uniquely defined in statistics (Capparelli et al., 2013), and calculated trends are method dependent (Franzke, 2012). There are multiple statistical approaches to estimating trends in time series and they must be carefully chosen and interpreted (Chang et al., 2021, 2023; Cooper et al., 2014, 2020; Gaudel et al., 2018), particularly when dealing with nonlinear and nonstationary data, with marked seasonality and interannual and decadal variability such as surface ozone at Tololo. As the climate system is complex, many processes interact with each other at multiple temporal and spatial scales leading to nonlinear responses to external and internal changes (Snyder et al., 2011; Wang et al., 2023). Intrinsic climate





variability plays an important role when assessing trends at the local and regional scales (Franzke, 2012). According to the same author, intrinsic climate variability leads to a so-called "stochastic trend" as it is expressed in autocorrelation (variables show temporal correlation), whereas a so-called "deterministic trend" emerges due to an external forcing. In general, detecting trends depends upon the size of the trend, the time span of available data, and the magnitude of variability and autocorrelation of the noise in the data (Weatherhead et al., 1998). In the case of atmospheric chemistry variables, one must add uncertainties derived from instrument detection level and sampling, change of sensors, the influence of extreme events, etc. (Chang et al., 2021).

The Tropospheric Ozone Assessment Report (TOAR) initiative has made a substantial contribution to standardizing the methods to visualize and calculate trends for data as those collected at Tololo. Hence, we use the Quantile Regression algorithm that allows piecewise detection of change points by Chang et al. (2023). Again, the concept of change point is not well-defined in statistics, nonetheless it is a useful indicator of significant changes in a time series over time, for instance change of instruments. In the case of Tololo, the ozone sensor was replaced in 2013 (Anet et al., 2017). We will assess whether this change is apparent in the data.

2.8 Generalized Additive Models for Tololo

Generalized Additive Models (GAMs) are an extension of linear models, allowing nonlinear and nonparametric fittings of complex dependences of response variables on explanatory variables. A GAM adopts a sum of arbitrary functions of variables —potentially nonlinear— that represent different features via splines, which altogether describe the magnitude and variability of the response variables (Hastie and Tibshirani, 1986; Molnar, 2025). The choice of explanatory variables is key. It must be based on physical reasoning about potential contribution of variables that one can logically expect to explain the response variable. Statistically, one should choose variables that contribute to explaining the response variable but are largely independent from one another (Kovács, 2024). Redundancy results in unstable parameter estimates in GAMs and makes the marginal effect of features harder to interpret. In the case of atmospheric variables, one cannot assure orthogonality among explanatory variables as they are generally autocorrelated, but an effort must be made to avoid redundancy. In this study, we applied expert knowledge, and partial dependence plots (Hastie et al., 2009) to assess the physical meaning and functional dependences of the estimated relationships and thereby interpreting the GAM results. Additionally, we used the SHapley Additive exPlanations (SHAP) approach –based on game theory— to determine the ranked contribution of each explanatory variable in GAM (Lipovetsky and Conklin, 2001). In a simplified manner, a GAM is of the form (Eq.1):

$$O_3 = \epsilon + f_1(v1) + f_2(v2) + \dots + f_N(vN)$$
 (Eq. 1)

where ϵ represents an error term, and f_i , i=1, N are spline functions of variables v_i , i=1, N (Hastie and Tibshirani, 1986; Molnar, 2025). The error term has a stochastic component, so we run our GAM 50 times. We utilized the following Python software: pyGAM available https://pygam.readthedocs.io/en/latest/ and shap available at https://shap.readthedocs.io/en/latest/.





3. Results and discussion

3.1 Change points and trend estimates

Seguel et al. (2024) analyze the ozone time series at Tololo over the period (1995-2021). They identify two change points in ozone, one in early 2006 and another in early 2014, both within uncertainties of several years. As the authors note, the 2006 change point coincides with the global increase in methane, also observed at Rapa Nui (Easter Island). In this work, we extend the analysis to include 2022 and 2023 and explore the role of several atmospheric variables. Thus, we repeat the change point analysis for ozone as well as for methane, temperature (T), specific humidity (q), dewpoint temperature (T_d), and geopotential height at 500 hPa (Z_{500}).

Methane was chosen due to its role as O_3 precursor in the background atmosphere (Crutzen, 1988; Crutzen et al., 1999). We included T because, in addition to typically explaining a significant part of the variance of near surface O_3 , key reactions leading to O_3 production depend on temperature (Pusede et al., 2015). Specific humidity was selected since the principal global sink of tropospheric O_3 is the photolysis by near ultraviolet radiation (λ < 310 nm) in the presence of water vapor (Jacob and Winner, 2009). We chose specific humidity instead of relative humidity to separate the effect of temperature from that of humidity. Dewpoint has been used as a meteorological explaining factor at Mauna Loa, allowing the separation between dry air associated with higher altitude and latitude air masses, and moist conditions associated with more tropical air masses, when applied to nighttime values avoiding upslope data (Gaudel et al., 2018). At Tololo, higher latitude air masses can be moist as they reach this subtropical site (30°S) in connection with deep troughs and cutoff lows (Fuenzalida et al., 2005; Rondanelli et al., 2002), while subtropical air masses are typically dry. Geopotential height at 500 hPa is used as an indicator of synoptic scale variability. These times series and their change points are illustrated in Figures 2 and 3.

Figure 2 shows the strong seasonality in O₃, CH₄ and CO. In addition to a marked seasonality, the most prominent characteristic of ozone is the maximum values that are observed in spring (Anet et al., 2017; Gallardo et al., 2000). Carbon monoxide also peaks in spring, except for some summer events. This maximum in ozone and CO is generally attributed to biomass burning (Anet et al., 2017; Daskalakis et al., 2022). But as we will see later, STE also plays a role in late winter and spring for ozone (Daskalakis et al., 2022; Rondanelli et al., 2002). The variability in methane, on the other hand, is less marked with a February-March minimum, and an August-September maximum, which is largely driven by the hydroxyl radical sink (East et al., 2024). ENSO also plays a role in methane interannual variability (Rowlinson et al., 2019), which will affect its seasonal variation too. The influence of ENSO, QBO, MJO has been found to be relevant for the variability of tropospheric ozone and its precursors (Daskalakis et al., 2022 and references therein).

Except for methane, change points calculated for all species are subject to multi-year uncertainties, which is to be expected given the relatively large variability of the time series (Muggeo, 2017), including long-term modes of variability (e.g., Pacific Decadal Oscillation, PDO) that may not be captured by the relatively short times series. The change point for ozone is estimated to occur near August 2005 with an uncertainty range between 2001 and mid-2010, which largely coincides with the upward acceleration of methane growth by mid-2006. The addition of the years 2022 and 2023 resulted in a sole



change point near 2006, instead of two as shown by Seguel et al. (2024). The near 2006 change is physically reasonable (methane) and consistent with the visual inspection of the time series. There is no evidence of an effect of the change of instruments in 2013. Interestingly, ozone shows a growing median trend both before and after 2006, the rate of growth being larger after 2006 than before 2006. The 5th and 95th percentiles indicate decreasing trends before 2006 and growing trends thereafter suggesting a more significant influence of extreme events in the later period.

In Figure 2, CO shows two points of change around 2009 and 2014, which, we hypothesize may be linked to an increased frequency and extent of fires in Central and Southern Chile (Carrasco-Escaff et al., 2024; González et al., 2018). However, we cannot rule out that the use of a combination of model and instrumental data may yield spurious results. Our fire hypothesis is based on the occurrence of large fires whose emissions of CO may reach Tololo, like in the summer of 2017 (Lapere et al., 2021).

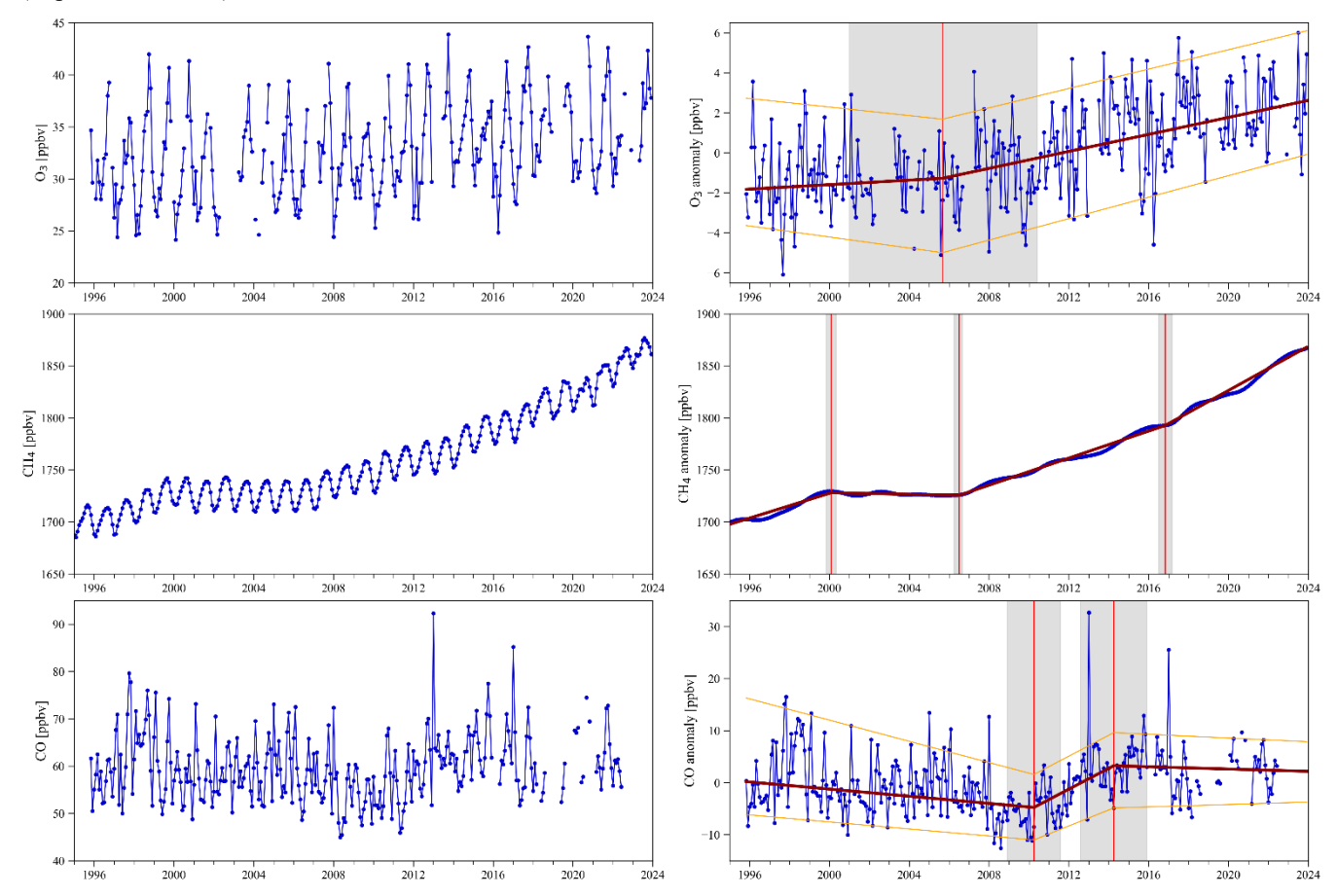


Figure 2. The left panels show the monthly time series of ozone measured at Tololo, and monthly time series of reconstructed (See text for details) methane (CH₄) carbon monoxide (CO). The right panels show the corresponding seasonal anomalies, and the deseasonalized smooth trend for methane. The dark red line indicates the trend of 50th percentile and the orange lines indicate the trends of 5th and 95th percentiles. The vertical red line indicates change detected points and the gray shaded area shows its 95% confidence interval.



Methane shows three change points around 2000, 2006 and 2016 (Cf. Figure 2). In late 1999 a plateau in CH₄ mixing ratios started, following a period of steady increase and that remained for a few years until late 2006. This was observed around the world but the reasons that explain these changes are still subject to debate due to the complex interactions between emissions and chemistry that drive atmospheric methane (Saunois et al., 2020). We identify a trend change in 2016 which coincides with observed but still not fully explained changes in CH₄ growth rate (Nisbet et al., 2019).

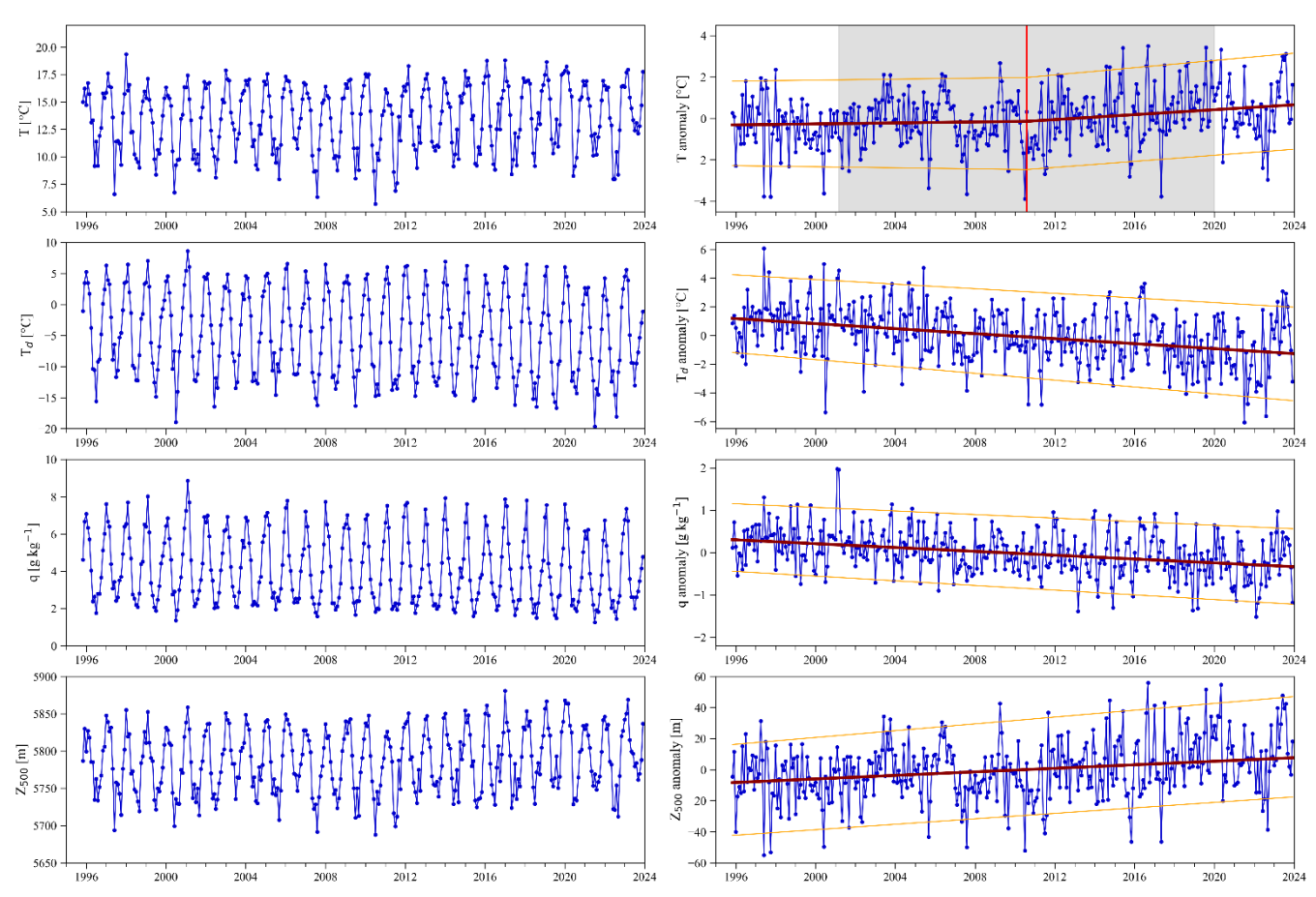


Figure 3. The left panels show monthly time series of temperature (T), dew point temperature (Td), specific humidity (q) and geopotential height in 500 hPa (Z500) provided by ERA5 reanalysis and corrected by in situ observations, when available (See text for details). The right panels show the corresponding anomalies for temperature, dew point temperature, specific humidity and geopotential height at 500 hPa. The dark red line indicates the trend of 50th percentile and the orange lines indicate the trends of 5th and 95th percentiles.

A strong seasonality in all meteorological variables is apparent in Figure 3. The strong contrast between summer and winter values is characteristic of the subtropics (Garreaud et al., 2009). Except temperature that shows a change point around 2010 but with a broad uncertainty span, none of the variables shown in Figure 3 show clear changes in trends. Nevertheless, Central and Southern Chile experienced a continuous drought from 2010 to 2022 (Garreaud et al., 2020), which was interrupted





by significant precipitation events over the latest winters. The changes in temperature and humidity observed at Tololo also reflect these conditions. This is in fact consistent with the warming and drying trends driven by climate change over Central and Southern Chile (Bozkurt et al., 2019).

As methane is the variable with the most noticeable upward trend, we assess the changes in hourly ozone distribution over time when methane changes. To this end, we consider four periods as inferred by the change points of methane. This is shown in Figure S 5. Until 2006, the mean and median of ozone only show a slight difference, while after 2006 these statistical indicators clearly increase. Moreover, the growth in the indicators appears to accelerate further after 2016. This suggests that methane is a major driver of ozone changes at Tololo.

Next, we provide an update of the trend estimate presented by Seguel et al. (2024), including the determination of change points, all according to TOAR II recommendations (Chang et al., 2023). This is shown in Table 1 and Figure 4. Table 1 shows that O₃ trends were negative or slightly positive before August 2005 for all percentiles, albeit with low reliability as defined by TOAR II. After the change point, a clear upward trend emerges for all percentiles (very high certainty). As previously indicated, trends at 5th and 95th percentiles are somewhat higher than the median trend, which may be indicative of the impact of extreme events, such as fires.

Table 1. Ozone trends and reliability (according to TOAR recommendation) are estimated for Tololo (5th, 50th (median) and 95th percentiles) over the period December 1995-December 2023. The table also shows year and month of the change point as well as the signal-to-noise ratio (SNR), the corresponding probability value (p Value), and the reliability of the estimate.

Percentile	Change Points	Trend ppbv / decade [± CI]	SNR	p Value	Reliability
5	Before August 2005	-1.4 [2.0]	-1.36	1.79E-01	Low certainty
50		0.4 [1.1]	0.85	3.97E-01	
95		-1.5 [2.9]	-1.06	2.94E-01	
5		2.7 [1.2]	4.54	3.11E-05	
50	After August 2005	2.1 [0.8]	4.85	1.07E-05	Very high certainty
95		2.5 [1.6]	3.11	2.93E-03	



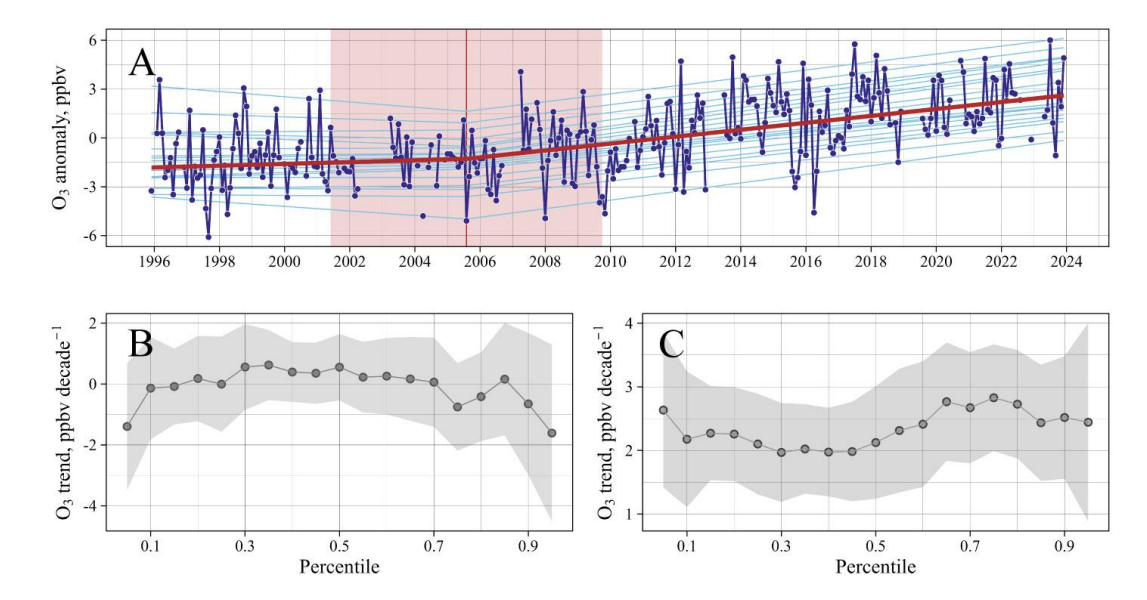


Figure 4. Percentile trends derived by quantile regression applied to the deseasonalized monthly surface ozone at Tololo. In panel (A), the blue dots and light lines show the monthly anomalies of ozone at Tololo, the red line corresponds to the trend of the 50th percentile, and the light blue lines correspond to the trends of the remaining percentiles. The change point is represented by a vertical red line, and the shaded red area shows the corresponding uncertainty at the 95% confidence interval. Panels (B), and (C) show the percentile trends of the quantile regression from the 5th to 95th percentiles at 5 percentile intervals before and after the change point, respectively.

3.2 Influence of stratospheric intrusions

We identified stratospheric intrusions as events of concurrent positive anomalies in ozone and negative anomalies in water vapor mixing ratio as described in Section 2.6. Using said method, we found 336 stratospheric intrusion events over the period 1995-2023, of which roughly half (170) last 24 hours or less, 122 (36%) last between 24 and 48 hours, 33 (10%) last between 48 and 72 hours, and 11 (5%) last more than 72 hours (Cf. Figure 5). Median anomalies in ozone are around 5 ppbv and -2 g/kg in water vapor, which are significant magnitudes compared with typical ozone and water vapor values at Tololo.

While stratospheric intrusion events can occur any month of the year, most of them take place during the cold season and early spring, between May and October. One can observe a distinct interannual variability in the number of events per year. Typically, there are fewer (more) intrusions in connection with the cold (warm) phase of ENSO, which is consistent with a stronger (weaker) South Pacific High that readily hinders (allows) the arrival of mid-latitude synoptic disturbances such as cutoff lows and deep troughs. There is no trend in the number of events per year nor in their duration. Furthermore, the number and duration of intrusion events do not appear to be related to the intensity of the ENSO anomaly (not shown).

At first sight, the fact that there are more intrusions in El Niño years might seem contradictory with the fact that the spring maximum in ozone at Tololo is typically larger during La Niña years rather than during El Niño years as firstly stated by Anet et al. (2017), and reproduced here (See Figure S 6). However, one must recall that stratospheric intrusions are not the only mechanism influencing ozone in Tololo.



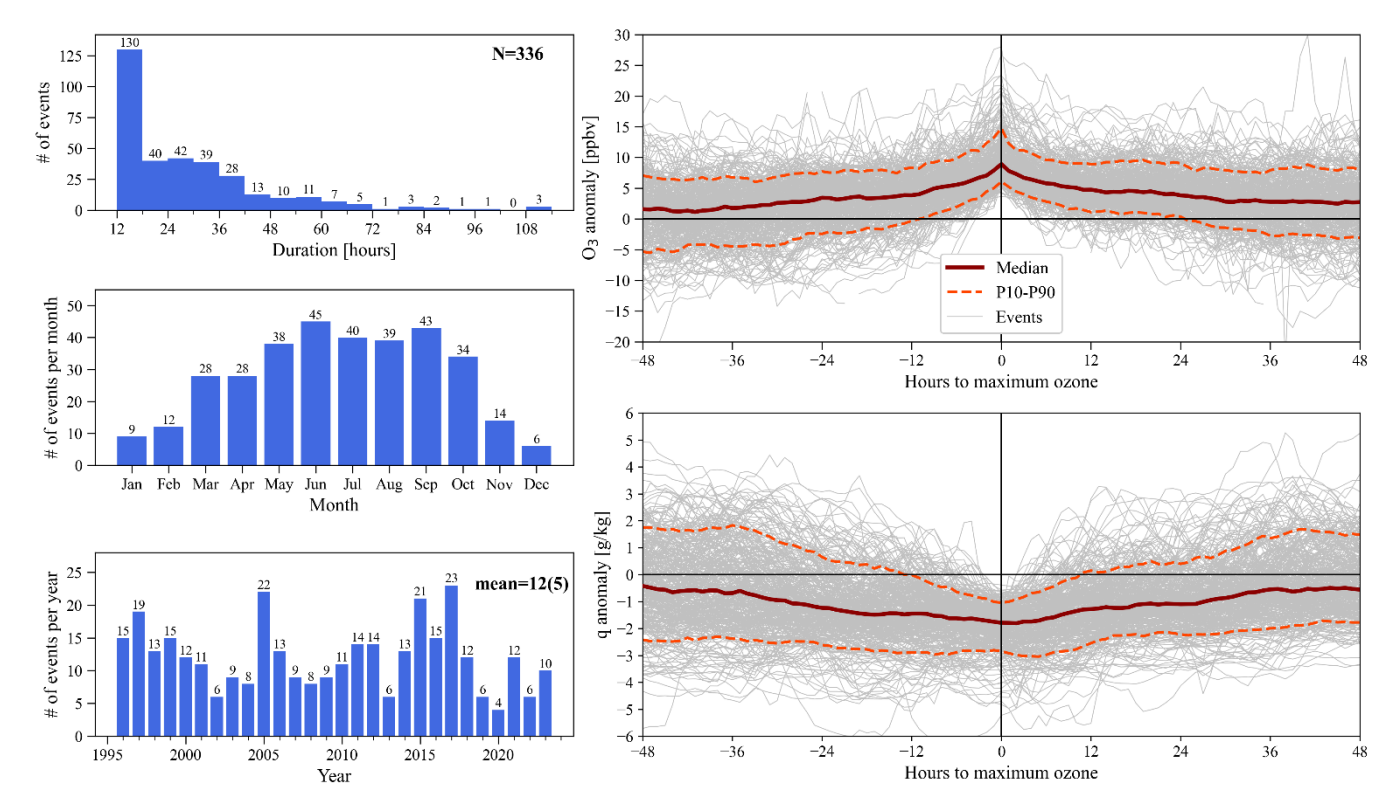


Figure 5. Stratospheric intrusion events as detected at Tololo according to anomalies in ozone (positive) and water vapor (negative). The upper left panel shows the number of events according to duration in hours. The middle-left panel describes the seasonal distribution considering all events occurring in each month. The bottom left panel indicates the number of events per year between November 1995 and December 2023. To the right we show the behavior of each intrusion (grey thin lines) as well as their statistics per percentile: 10 (dashed orange line), 50 (dark red line) and 90 (dashed orange line). The upper (lower) right panel shows the statistics for ozone (water vapor mixing ratio).

In addition to counting intrusion events, we characterized their synoptic scale evolution. Figure 6 and 7 show composite anomalies in synoptic meteorological fields over a 12-day period that starts 10 days prior and ends 2 days after the stratospheric intrusion event. In the horizontal we show composite anomalies in geopotential height at 500 hPa, and vertical velocity (Figure 6). These fields show a slow passing deep trough of north-west to south-east orientation that reaches north of 30°S 10-days prior and shows a full mature stage by day -4. While the trough is approaching the Chilean coast, one observes uplifting (subsidence) west (east) of the Andes, which is consistent with the behavior of deep troughs and cutoff lows (Rondanelli, 2025). Thereafter, a subsidence zone is evident and advances eastward from day -2 to day 0, while a ridge develops and the subtropical high-pressure system is re-established. Thus, there is subsidence upwind and passing over Tololo with vertical velocity anomalies of more than 0.15 Pa/s, i.e., producing favorable conditions for stratospheric ozone mixing down to Tololo.





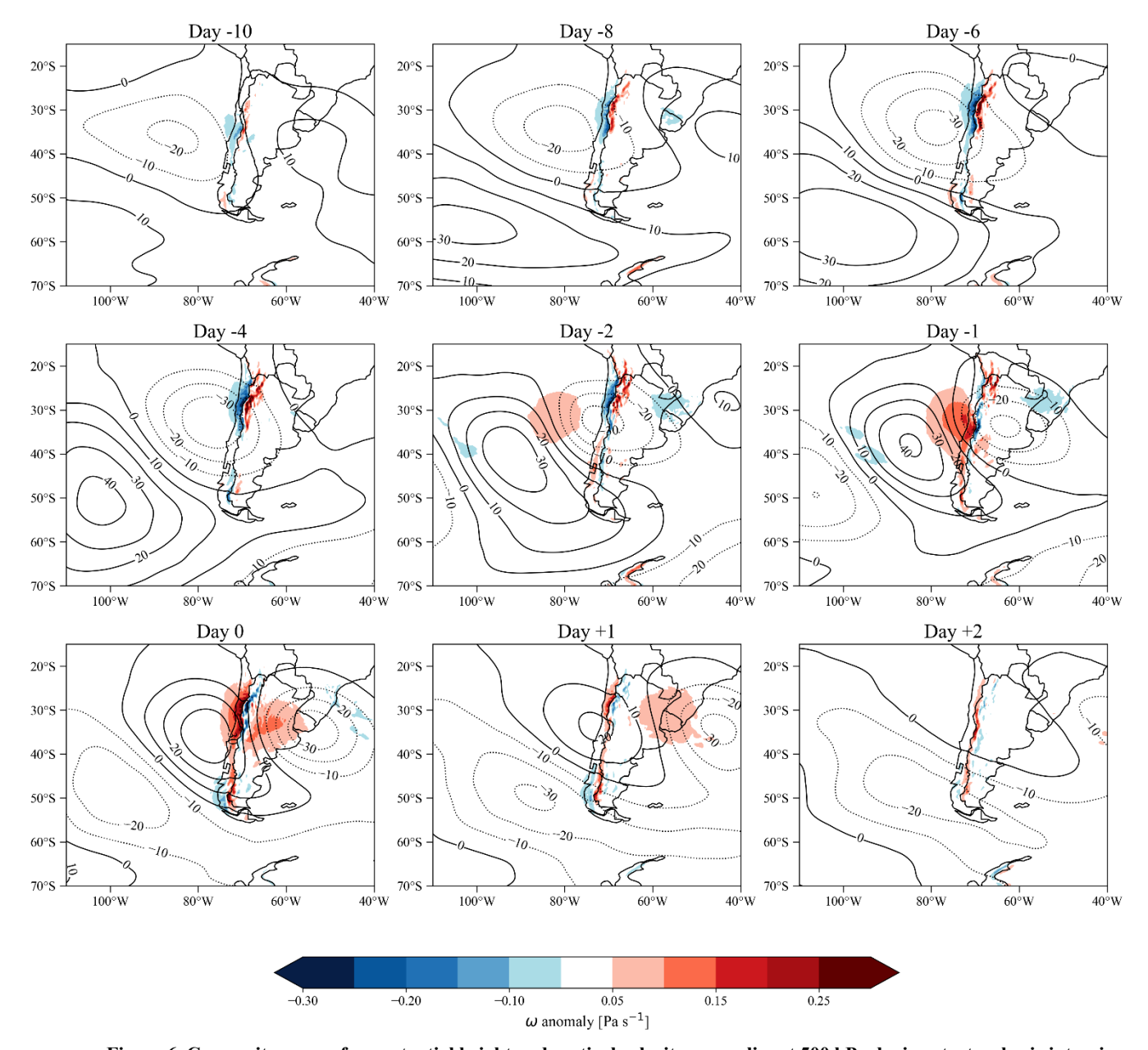


Figure 6. Composite maps of geopotential height and vertical velocity anomalies at 500 hPa during stratospheric intrusion events. Contours denote geopotential height anomalies in meters, where positive (negative) anomalies are solid (dotted) contours. Shaded areas denote vertical velocity anomalies in Pa/s.





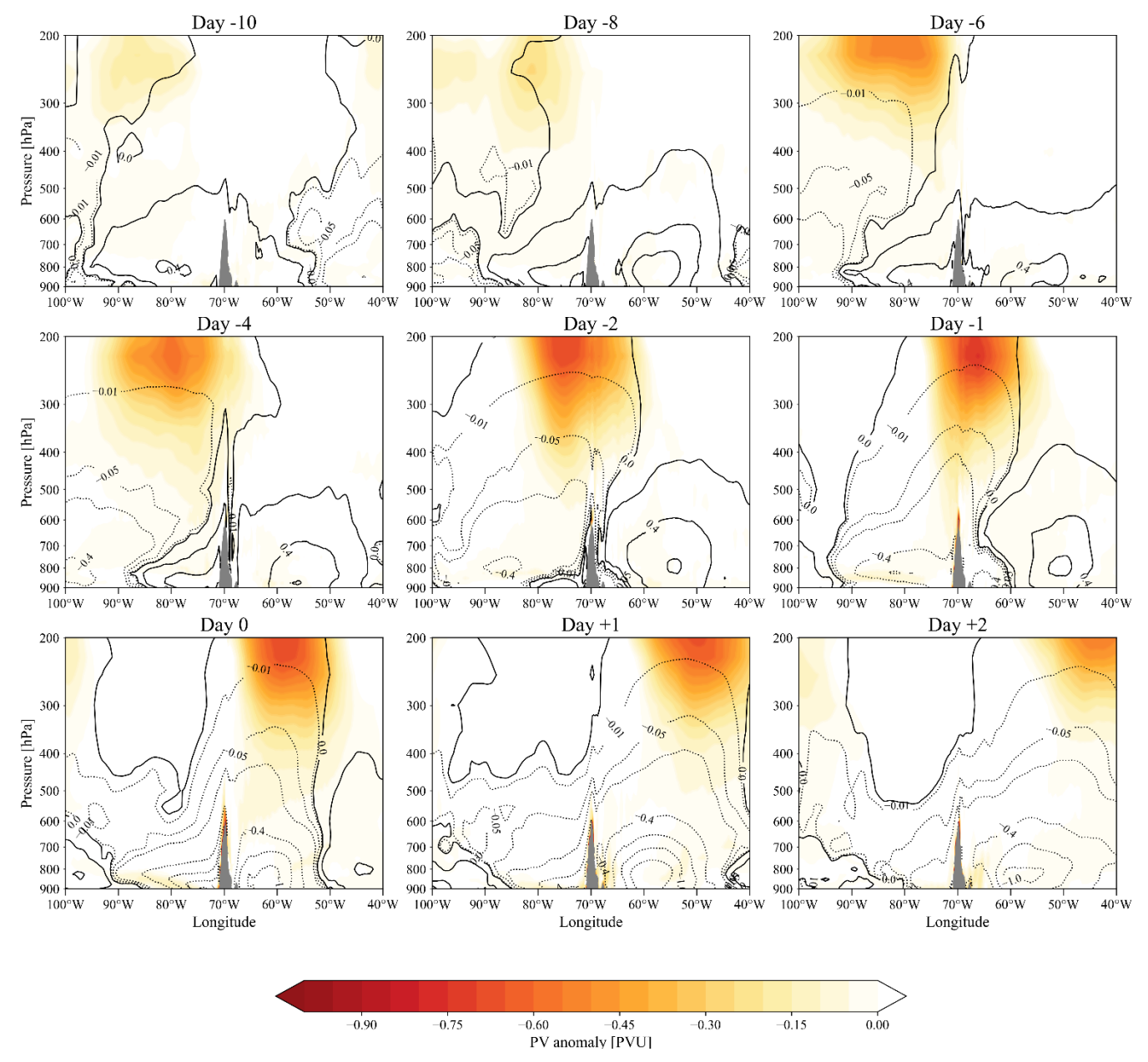


Figure 7. Composite of longitude-pressure cross-section of potential vorticity and specific humidity anomalies between 900 and 200 hPa during stratospheric intrusion events. Contours denote specific humidity anomalies in g/kg, where positive (negative) anomalies are solid (dotted) contours. The shaded area denotes potential vorticity anomalies in potential vorticity units (PVU).

3





It is well known that stratospheric air is characterized by negative vorticity, and low humidity. Therefore, in Figure 7, we show composite anomalies of potential vorticity and specific humidity of stratospheric intrusion events. Consistently with the synoptic patterns discussed in Figure 6 but occurring ca. 48 hours prior, the development of the deep trough is accompanied by the entrance of negative anomalies of potential vorticity and humidity that propagate downwards, starting to reach Tololo already by day -2, i.e., prior to the maximum ozone and humidity anomalies. This is consistent with the duration of the events that typically last less than 3 days (>80% of the cases). Thereafter, the intruding air follows the westerlies with continued negative anomalies in potential vorticity and humidity east of the Andes.

Hence, based on the observed data, stratospheric intrusions events lead to increases in ozone of around 5 ppbv on average at Tololo within a range between 3 and 12 ppbv, accompanied by negative anomalies in humidity of around -2 g/kg, which in turn compare with typical ozone and water vapor mixing ratios of 30 ppbv and 7 g/kg, corresponding to 17% and 28% respectively. Such events occur mainly in the cold season and early spring and are favored by El Niño conditions. Said intrusions typically occur in connection with deep troughs and cutoff lows that connect the subtropics with higher latitudes. On average, one finds 12 events per year but within a broad range between 4 and 23 events per year.

The TM4-ECPL model also provides an estimate of the stratospheric influence on Tololo ozone (Figure 8). In these simulations, the ozone of stratospheric origin reaches Tololo all year around but in winter and early spring (June through September) this contribution surpasses 10 ppbv (on average), and in summer (December through February) it is roughly half of that. This corresponds to a percentage contribution of roughly 15% in summer to 25% in winter. It is worth noting that the seasonality of the stratospheric contribution found in the simulations is largely consistent with the seasonality found through our methodology and shown in Figure 5, i.e., the model captures the overall seasonal variability of ozone with higher values in winter and early spring than in summer and early fall. However, an overestimate of ozone at Tololo by nearly a factor of two is evident. Moreover, there are many days with stratospheric contributions that reach or surpass 50% of the estimated ozone in winter (Cf. Figure 8). We suspect that part of the mismatch between model and observations is due to too strong a stratospheric contribution. In its current version, the upper boundary condition for O₃ is estimated by nudging O₃ concentrations above 50 hPa altitude to satellite observations with no explicit stratospheric chemistry. This was already reported when evaluating TM4-ECPL against ozone soundings at Rapa Nui, where an overestimate of ozone in the upper troposphere was found (Daskalakis et al., 2022).

In Figure 9 we show the number of days of stratospheric intrusions and their contribution to ozone as calculated by TM4-ECPL for the period 1995-2015, categorized by season. Also, we indicate the number of events that coincide with those detected by our empirical methodology. The total number of days estimated by TM4-ECPL is typically an order of magnitude higher than the number of days when stratospheric intrusions were detected, particularly in summer, which again suggests too strong a stratospheric contribution all year. Also, TM4-ECPL estimates many days with stratospheric contributions of less than 5 ppbv, whereas the concurrently observed intrusions do not. The largest stratospheric contributions estimated by TM4-ECPL reach 40 ppbv or 35 ppbv when considering only days when we observed intrusions, which is in any way much larger than the



2

3

4 5 6

7



ozone anomalies based on the empirical method that reaches up to 25 ppbv. Lastly, the median stratospheric contributions calculated with TM4-ECPL are around 15 ppbv per day but that of the empirical method is only 5 ppbv.

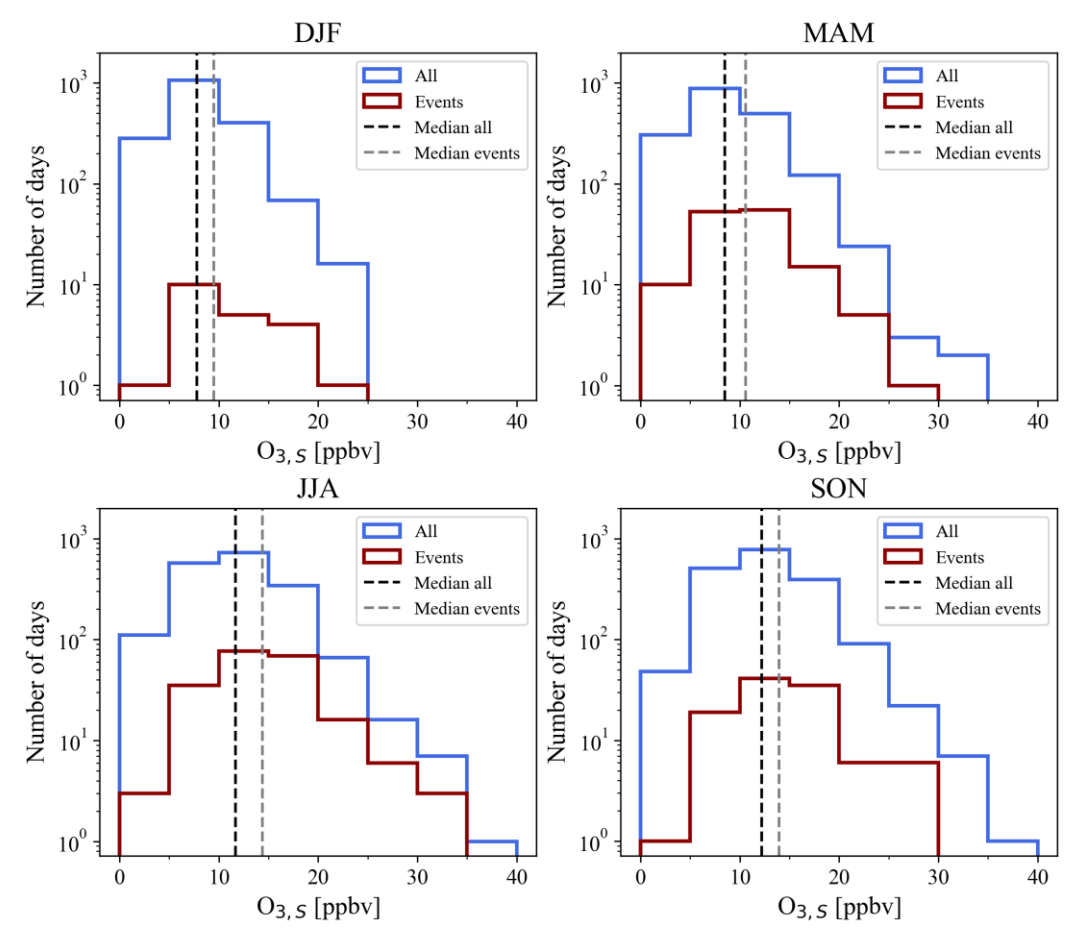


Figure 9. Seasonal daily stratospheric ozone contributions (O₃,s) at Tololo according to the TM4-ECPL model. In blue we show the distribution of all events calculated by the model. In red, we show the events that coincide with intrusion events as determined by the empirical methodology. Each panel shows the corresponding histogram for summer (DJF), fall (MAM), winter (JJA) and spring (SON). Vertical dashed lines indicate the median of the distributions.

3.3 Influence of biomass burning

As shown in Figure S 4, CO at Tololo was overestimated by the model simulation by on average about 7 ppbv over the period when we count with both observations and simulations (2013-2015). We corrected this by applying a bias correction method (Cannon et al., 2015; Staehle et al., 2024) to reconstruct the whole model series (1995-2015). The contribution of biomass burning to CO and ozone was calculated as the difference between the runs with and without biomass burning as shown in Figure 10. The role played by biomass burning in terms of ozone production and transport over the east Pacific – particularly during spring—has been shown in earlier work (e.g., Daskalakis et al., 2022). This influence is also clear in Tololo where an increase in CO during spring is both simulated and observed (See Figure S 2). While observations of CO do not





allow attributing the biomass signal, simulations do. According to the TM4-ECPL model outputs, i.e., with all sources and without biomass burning, the seasonally averaged contribution to ambient CO at Tololo reaches up to nearly 23% in October. The minimum contribution occurs in April when the average it is about 5%. Notice that in summer (DJF), averaged values of biomass burning contributions are lower than in spring, but one observes a secondary maximum in connection with regionally occurring fires that have become more common over central and southern Chile (e.g., Lapere et al., 2021). Regarding ozone, the biomass contribution peaks also in October, but it only reaches a median value of about 15% of total ozone (~35 ppbv).

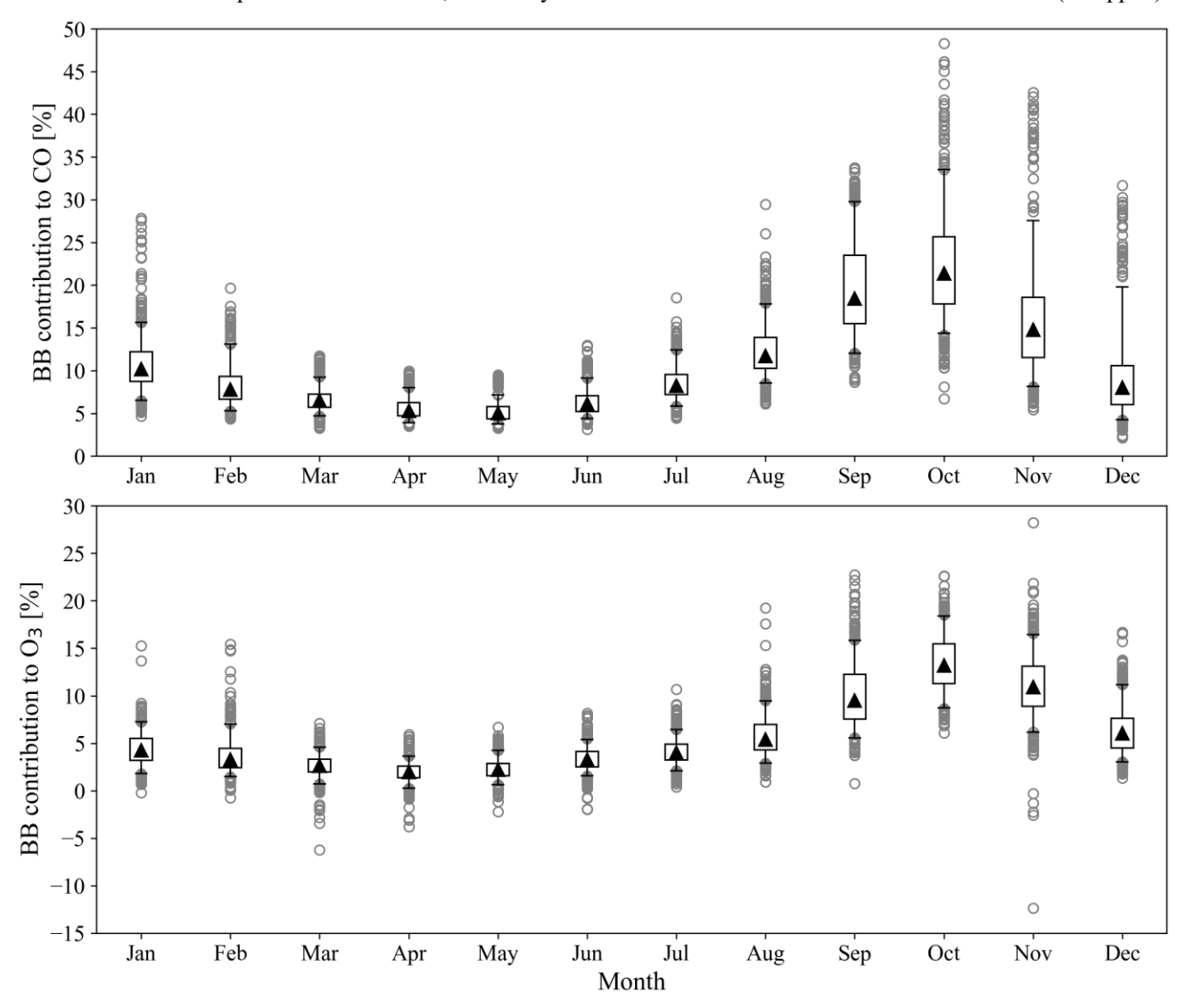


Figure 10. Biomass burning (BB) contribution to CO (upper panel) and ozone (lower panel) as calculated by the TM4-ECPL model. Monthly averages are calculated over daily values. Whiskers indicate the 5th and 95th percentiles of the data distributions. Outliers are shown as grey circles.





3.4 GAM model

After trying several combinations of potential explanatory variables, we chose 14 as indicated in Table 2. This set of variables were chosen based on their physical meaning and relevance for explaining ozone and trying to identify largely independent variables. Thus, our GAM has the general expression (Eq. 2):

$$O_3 = \epsilon + f_1(T) + f_2(q) + f_3(v) + f_4(Wdir) + f_5(BLH) + f_6(STE\ duration) + f_7(ENSO) + f_8(QBO) + f_9(MJO) + f_{10}(\omega) + f_{11}(CH_4) + f_{12}(CO) + f_{13}(DofW) + f_{14}(DofY)\ (Eq.\ 2)$$

where ε represents an error term, and f_i , i=1,14 are spline functions, in this case with 9 nodes that represent the dependences – potentially nonlinear— on different variables detailed in Table 2.

The model (GAM) aims at capturing daily average values of ozone. As seen in Figure 11, the model represents most features of the time series, including day-to-day, seasonal and interannual changes. It captures 76% of the data variability but it tends to underestimate extreme values. Still, on average, the error is less than 3.6 ppbv. Also, the model captures the trend of the observed data, i.e., 1.0 ppbv/decade, using the Ensemble Empirical Mode Decomposition (EEMD) as described in Anet et al. (2017). This trend is 30% larger than the one calculated by Anet et al. (2017), which is in line with increasing ozone mixing ratios at Tololo. When we run GAM without considering the influence of methane, GAM estimates a trend for the 1996-2023 period of only 0.4 ppbv/decade, highlighting the significant role of methane in explaining the observed upward trend in ozone at Tololo. Without methane both variance (74%) and error (3.7) show a slightly worse performance.

To assess the relative importance of the different variables we used two techniques. First, we calculated the partial dependences of the GAM reconstructed ozone with respect to each variable. This is shown in Figure 12, and discussed here:

- The day of the year (seasonality) contributes the most to ozone with up to 8 ppbv in spring, and secondarily with ca. 3 ppbv in winter. Seasonality also contributes slightly (< 2 ppbv) but negatively to ozone at Tololo in fall. In summer, a small increase in ozone appears. This seasonal variability is fully consistent with the processes we have previously described: STE in winter and spring, biomass burning in spring, episodical fires over central and southern Chile in summer, etc.
- The second largest contributing variable is absolute humidity. This relationship is inversely proportional between O₃ and humidity, reflecting the fact that water vapor acts as a sink for ozone, particularly in the remote atmosphere. While dry air is associated with higher ozone levels, wet air of marine origin is associated with lower ozone levels. The former is consistent with the influence of free tropospheric air, potentially of stratospheric origin, which is typically linked to dry or very dry air. The latter occurs in summer when the marine boundary layer grows, entraining wet and low ozone air, or when deep troughs and sometimes cutoff lows reach the subtropics vigorously mixing up wet air.
- Regarding the influence of temperature, we find that low values (<5 °C) result in a negative contribution possibly linked to very stable atmospheric conditions including subzero temperatures and very stable conditions leading to dry deposition. Higher temperatures (>5°C) show a positive relationship, largely linear with a contribution of up to 4 or 5 ppbv in ozone. This type of relationship has been found in many places around the world in polluted areas and they are attributed to the





- increase of reaction rates with temperature, as well as to more intense solar radiation and increases in biogenic VOC emissions (Porter and Heald, 2019; Szopa, 2021). At Tololo, such phenomena cannot be ruled out however the magnitude of the relationship is much smaller than the one found in the polluted conditions of Santiago (not shown). Moreover, the graph showing the day of the week shows no significant changes in ozone during the week, in other words there is no weekend-effect as typically found in urban areas and suggestive of local ozone precursors (Seguel et al., 2012).
- Boundary layer height has a clear positive influence on ozone up to 400 m, thereafter its impact declines and becomes negative for heights above 800 m. A growing boundary layer may result in the downward mixing of O₃ rich air from the free troposphere, however too deep a boundary layer is suggestive strong vertical mixing and intrusion of marine air that is typically O₃ poor, a phenomenon already described in connection with the description of the effects of humidity.
- A distinct although somewhat noisy positive contribution to O₃ is attributed to the duration of stratospheric intrusions as
 defined in this work, which is to be expected under those circumstances. A similar result was found when using potential
 vorticity: the more negative (more stratospheric) it is, the larger the contribution to O₃. To avoid including two equivalent
 indicators, we decided to include the simpler duration indicator.
- Our ENSO indicator (MEI) has overall a positive impact on ozone, and more markedly so during La Niña years. In connection with La Niña years, one expects stronger subsidence able to transport upper ozone rich air towards Tololo.

 During El Niño years, the subtropical high is weakened, and more synoptic systems may arrive at Tololo. Thus, despite the noisiness of the relationship between ozone and MEI, it appears physically sound.
 - Variability sources like QBO and MJO show a minor contribution (< 2ppbv) to O₃. The phase of MJO shows a rather discrete maximum at phase 5 which is largely consistent with the observations by Barrett et al. (2012), who found a maximum in ozone for phase 6 of MJO in Santiago, i.e., still in the subtropics of Chile. This coincides with active convection over the western Pacific and a strengthened Pacific high over the eastern Pacific. The influence of QBO appears to be small with relative maxima with either Westerly or Easterly winds in the stratosphere. This might be because Tololo is only at 2151 m a.s.l., which makes it difficult for a stratospheric signal to be clearly distinguished. Still, one must keep in mind that when contributions are small there is the risk of over-interpreting potential statistical artifacts.
 - Wind direction shows a positive contribution (up to 1 ppbv) that is maximized on westerly winds (250 degrees) that bring air from the Pacific that in spring transports the biomass signature that is rich in O₃ and O₃ precursors. Also, northerly winds show a maximum that may occur in connection with midlatitude disturbances that are often associated with subsidence behind the low-pressure system and sometimes tropopause breaks. However, these contributions are small, and they might be statistical artifacts. The dependence on wind speed is rather flat over the range between 0 and 12.5 m/s, but slightly positive, which again might be linked to the passage of synoptic disturbances and their associated vertical mixing.
 - Positive omega velocity (subsidence) shows a relatively small (< 2 ppbv) influence on O₃, which is expected as the free troposphere is generally richer in ozone than the lower troposphere. However, negative omega velocities also show a minor positive contribution to O₃. This may be linked to the subsiding back side of synoptic perturbations.





- According to our GAM, methane contributes positively to ozone with CH₄ mixing ratios above ~1725 ppbv, and slightly negative below that value, which roughly coincides with the first methane change point shown in Figure 2. There is an inflexion point in the contribution when methane surpasses 1780 ppbv and approaching 1800 ppbv the contribution increases to nearly 3ppbv with current methane levels. Again, this coincides with the change points of the methane time series (Cf. Figure 2). This is consistent with what we have discussed regarding the role of methane in explaining the trend observed in ozone at Tololo.
- CO shows a positive contribution above 75 ppbv, which coincides with the value observed in spring and linked to biomass burning transported over the Pacific. Above that level, the contribution of CO increases further.

Notice that all 50 runs of GAM showed similar functional dependences of the variables (See Figure 11) except for different error distributions among different variables. Thus, while the quantitative functional dependences may vary among runs, there is an overall physical consistency in those.

Table 2. Chosen variables for GAM to explain ozone at Cerro Tololo. For sources of information and data please see the main text.

Variable	Symbol	Units	
Local Meteorology (at 775 hPa)			
Temperature	T	Degrees Celsius (°C)	
Specific Humidity	q	g/kg	
Wind speed	v or Wind speed	m/s	
Wind direction	Wdir or Wind direction	Degrees	
Boundary layer height	BLH	m	
Vertical velocity	ω	Pa/s	
Synoptic Meteorology			
Duration of STE	STE Duration	h	
Large-scale variability		PVU	
El Niño/La Niña Southern	MEI		
Oscillation			
Quasi Biennial Oscillation at 50	QBO	Nondimensional	
hPa			
Madden-Julian Oscillation Phase	MJO	Nondimensional	
Atmospheric Composition in situ			
Observed methane combining Rapa	CH ₄	ppbv	
Nui and Tololo series			
Carbon monoxide combining (bias	CO	ppbv	
correction) TM4-ECPL and observations			
Temporal variables			
Day of the week	D-W	Nondimensional	
Day of the year	D-Y	Nondimensional	





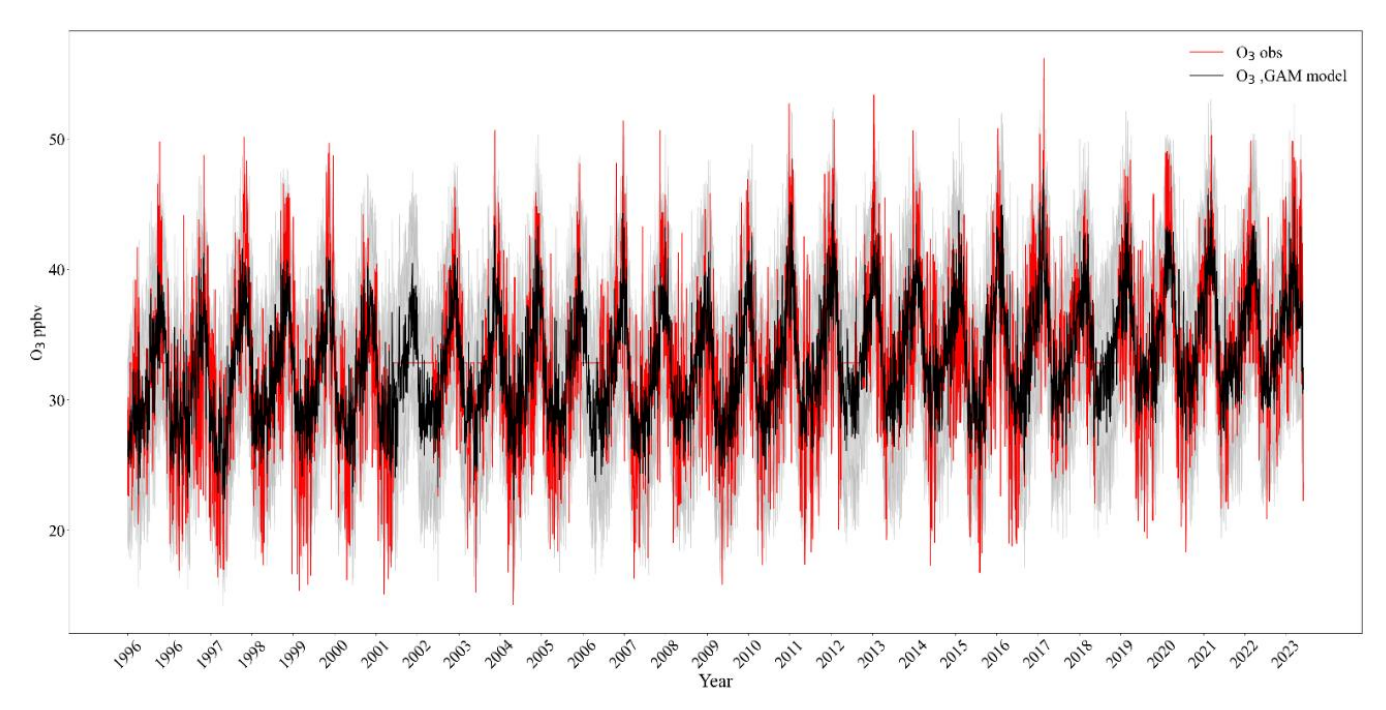


Figure 11. Reconstruction of the ozone time series through GAM as described in the text. The red values are daily averaged observations, and the black ones are those of the GAM model. The grey line shows the 5th and 95th confidence intervals.

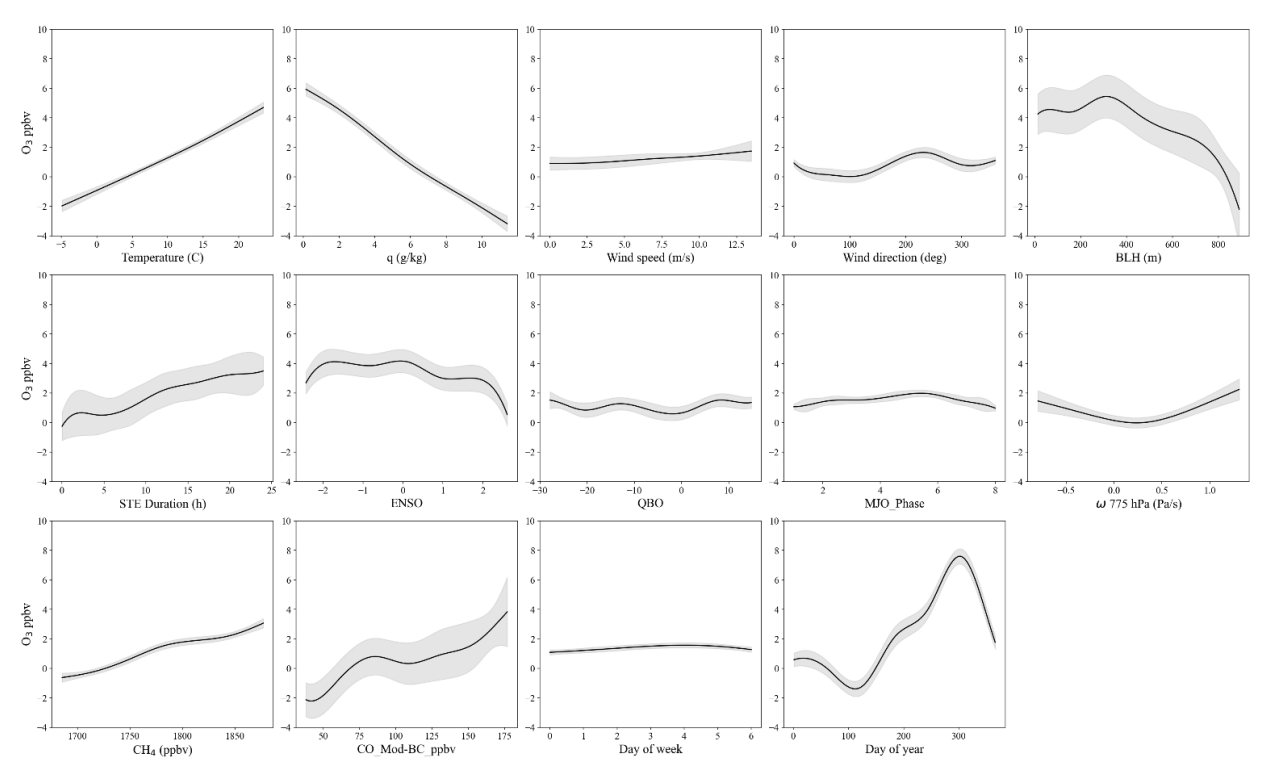


Figure 12. Partial dependences of the GAM reconstructed ozone on each variable.





The previous paragraphs describe the partial dependences found in GAM. Now we present the results of the SHAP method (See Figure S 7). Again, SHAP ranks seasonality, humidity, temperature, methane, carbon monoxide, and boundary layer height as the most important variables, following the physical reasoning described earlier. The same applies for the duration index. However, according to SHAP, El Niño years have mostly a negative influence on ozone, while La Niña years have a slight positive impact, which differs somewhat from the much smoother ENSO functional dependence shown in Figure 12. All other remaining variables are of less importance in SHAP. All in all, despite minor differences, the partial dependences of the GAM and the SHAP approach result in similar results in terms of the relative importance and role of the independent variables affecting ozone. This is encouraging as these methods have different mathematical grounds.

4. Summary and conclusions

In this work, we have studied ozone trends and variability at Tololo in the subtropics (mainly in the free troposphere) of the Southern Hemisphere. We used the TOAR methodological recommendations to detect change points and estimated linear trends per percentile between change points for ozone as well as for methane, temperature, specific humidity, dewpoint temperature, and geopotential height at 500 hPa which are potential explanatory variables for O_3 . Ozone shows a growing median trend both before and after 2006, the rate of growth being larger after 2006 (2.1 \pm 0.8 ppbv/decade, very high certainty) than before 2006 (0.4 \pm 1.1 ppbv/decade, low certainty). The 5th and 95th percentiles indicate decreasing trends before 2006 and growing trends thereafter suggesting a more significant influence of extreme events in the later period.

Of all potential explanatory variables for ozone included in our GAM, methane accounts for the growing trend in ozone. This is also suggested by the concurrent changes in ozone and methane over the period 1996-2023 (Figure S 5). While this has been indicated in earlier work, our GAM approach provides a quantitative assessment of the association.

Knowing that stratospheric intrusions are characterized by relatively high O₃ and low water vapor mixing ratios, we used the hourly anomaly time series of O₃ and specific humidity at Tololo to identify said intrusions. We found 336 stratospheric intrusion events over the period 1995-2023, of which roughly half (170) last 24 hours or less, 122 (36%) last between 24 and 48 hours, 33 (10%) last between 48 and 72 hours, and 11 (5%) last more than 72 hours (Cf. Figure 5). The composite patterns of these events coincide with the approach of cutoff lows and deep troughs. Hence, based on the observed data, stratospheric intrusions events lead to increases in ozone of around 5 ppbv (3 to 12 ppbv) on average at Tololo, accompanied by negative anomalies in humidity of around -2 g/kg, which in turn compare with typical ozone and water vapor mixing ratios of 30 ppbv and 7 g/kg, i.e., 17% and 28% respectively. While stratospheric intrusion events can occur any month of the year, most of them take place during the cold season and early spring, between May and October. Typically, there are more intrusions in connection with the warm phase of ENSO, which is consistent with a weaker South Pacific High, allowing the arrival of mid-latitude synoptic disturbances such as cutoff lows and deep troughs. There is no trend in the number of events per year nor in their duration. The influence of stratospheric air was also assessed using a state-of-the-science atmospheric chemistry model (TM4-ECPL). The model captures the seasonal variability in the stratospheric ozone





contribution, but it calculates too strong an impact, possibly due to the way it handles the upper boundary condition as identified in an earlier study.

According to the bias corrected TM4-ECPL model outputs, i.e., with all sources and without biomass burning, the seasonally averaged contribution to ambient CO at Tololo reaches up to 23% in October. The minimum contribution occurs in April when the average it is about 5%. In summer, averaged values of biomass burning contributions are lower than in spring, but one observes a relative maximum in connection with regionally occurring fires that have become more common over central and southern Chile. The contribution of biomass burning to ozone peaks also in October, but it only reaches a median value of about 15% of total ozone or about 5 ppbv. Hence, the contributions of biomass burning and stratosphere-to-troposphere transport on O₃ at Tololo, particularly during the late winter and spring ozone maximum are of similar magnitude and in the order of 5 ppbv per event, with a broad range of variability.

To follow changes in atmospheric composition and ozone forcing in the free troposphere of the otherwise sparsely observed Southern Hemisphere, Tololo has privileged location. It is typically immersed in the free troposphere and affected by the subsidence regime of the South Pacific high that brings clear sky conditions, and in winter, the subtropical jet stream is located on average at 30°S. In a rapidly changing climate, the expected intensification and expansion of the Hadley, and possibly Walker, circulation can be followed from Tololo not only in terms of meteorological variables but through the radiatively relevant ozone and methane. Thus, we argue that Tololo is a key background station to maintain and expand in the context of a rapidly changing climate.

19 A

Author contributions. LG, ChO, CM: conceptualization; ND, MK atmospheric chemistry simulations; ChO, RR: composite analysis; ChO, LC: Trend analysis; CM, LG: GAM methodology; CHO, KB, LG bias correction; ChO data curation; LG: writing of original draft; All authors: writing, review and editing.

Acknowledgements. Thanks to the Chilean Weather Office for keeping up and running the Tololo station, particularly to meteorologist Luis Valle. Technical support from engineer Sebastian Villalón is acknowledged. The first author made limited use of https://researchassistant.nature.com/ to improve the clarity of the text. Maria Kanakidou gratefully acknowledges the support received from the U Bremen Excellence Chair Program.

Financial support. Chilean researchers received support from FONDAP/ANID 1523A0002. The atmospheric chemistry simulations were partly performed on the HPC cluster *Aether* at the University of Bremen, financed by the Deutsche Forschungsgemeinschaft (DFG, German Research Foundation) under Germany's Excellence Strategy (University Allowance, EXC 2077, University of Bremen).





References

1

- 2 Ainsworth, E. A.: Understanding and improving global crop response to ozone pollution, Plant Journal, 90, 886–897, 3 https://doi.org/10.1111/tpj.13298, 2017.
- 4 Anet, G. J., Steinbacher, M., Gallardo, L., Velásquez Álvarez, A. P., Emmenegger, L., and Buchmann, B.: Surface 5 ozone in the Southern Hemisphere: 20 years of data from a site with a unique setting in El Tololo, Chile, Atmos Chem Phys, 6 17, 6477–6492, https://doi.org/10.5194/acp-17-6477-2017, 2017.
- 7 Barrett, B. S., Fitzmaurice, S. J., and Pritchard, S. R.: Intraseasonal variability of surface ozone in Santiago, Chile: 8 Madden-Julian Oscillation Modulation by phase of the (MJO), Atmos Environ. 57, 55-62, 9 https://doi.org/10.1016/j.atmosenv.2012.04.040, 2012.
- 10 Bourgeois, I., Peischl, J., Neuman, J. A., Brown, S. S., Thompson, C. R., Aikin, K. C., Allen, H. M., Angot, H., Apel,
- 11 E. C., Baublitz, C. B., Brewer, J. F., Campuzano-Jost, P., Commane, R., Crounse, J. D., Daube, B. C., DiGangi, J. P., Diskin, G. S., Emmons, L. K., Fiore, A. M., Gkatzelis, G. I., Hills, A., Hornbrook, R. S., Huey, L. G., Jimenez, J. L., Kim, M., Lacey,
- 13 F., McKain, K., Murray, L. T., Nault, B. A., Parrish, D. D., Ray, E., Sweeney, C., Tanner, D., Wofsy, S. C., and Ryerson, T.
- 14 B.: Large contribution of biomass burning emissions to ozone throughout the global remote troposphere, Proceedings of the
- 15 National Academy of Sciences, 118, https://doi.org/10.1073/pnas.2109628118, 2021.
- 16 Bozkurt, D., Rojas, M., Boisier, J. P., Rondanelli, R., Garreaud, R., and Gallardo, L.: Dynamical downscaling over 17 the complex terrain of southwest South America: present climate conditions and added value analysis, Clim Dyn, 53, 6745-18 6767, https://doi.org/10.1007/s00382-019-04959-y, 2019.
- 19 Cannon, A. J., Sobie, S. R., and Murdock, T. Q.: Bias Correction of GCM Precipitation by Quantile Mapping: How 20 Well Do Methods Preserve Changes in Quantiles and Extremes?, J Clim, 28, 6938-6959, https://doi.org/10.1175/JCLI-D-14-21 00754.1, 2015.
- 22 Capparelli, V., Franzke, C., Vecchio, A., Freeman, M. P., Watkins, N. W., and Carbone, V.: A spatiotemporal analysis 23 of U.S. station temperature trends over the last century, Journal of Geophysical Research Atmospheres, 118, 7427-7434, 24 https://doi.org/10.1002/jgrd.50551, 2013.
- 25 Carrasco-Escaff, T., Garreaud, R., Bozkurt, D., Jacques-Coper, M., and Pauchard, A.: The key role of extreme 26 weather and climate change in the occurrence of exceptional fire seasons in south-central Chile, Weather Clim Extrem, 45, 27 100716, https://doi.org/10.1016/j.wace.2024.100716, 2024.
- 28 Chang, K. L., Schultz, M. G., Lan, X., McClure-Begley, A., Petropavlovskikh, I., Xu, X., and Ziemke, J. R.: Trend 29 detection of atmospheric time series: Incorporating appropriate uncertainty estimates and handling extreme events, 30 https://doi.org/10.1525/elementa.2021.00035, 15 December 2021.
- 31 Chang, K.-L., Schultz, M. G., Koren, G., and Selke, N.: Guidance note on best statistical practices for TOAR analyses, 32 2023.





- 1 Checa-Garcia, R., Hegglin, M. I., Kinnison, D., Plummer, D. A., and Shine, K. P.: Historical Tropospheric and Stratospheric Ozone Radiative Forcing Using the CMIP6 Database, Geophys Res Lett, 45, 3264-3273, 2 3 https://doi.org/10.1002/2017GL076770, 2018.
- 4 Christiansen, A., Mickley, L. J., Liu, J., Oman, L. D., and Hu, L.: Multidecadal increases in global tropospheric ozone 5 derived from ozonesonde and surface site observations: Can models reproduce ozone trends?, Atmos Chem Phys, 22, 14751– 6 14782, https://doi.org/10.5194/acp-22-14751-2022, 2022.
- 7 Clifton, O. E., Fiore, A. M., Massman, W. J., Baublitz, C. B., Coyle, M., Emberson, L., Fares, S., Farmer, D. K.,
- 8 Gentine, P., Gerosa, G., Guenther, A. B., Helmig, D., Lombardozzi, D. L., Munger, J. W., Patton, E. G., Pusede, S. E.,
- 9 Schwede, D. B., Silva, S. J., Sörgel, M., Steiner, A. L., and Tai, A. P. K.: Dry Deposition of Ozone Over Land: Processes,
- 10 Measurement, and Modeling, https://doi.org/10.1029/2019RG000670, 1 March 2020.
- 11 Cooper, O. R., Parrish, D. D., Ziemke, J., Balashov, N. V., Cupeiro, M., Galbally, I. E., Gilge, S., Horowitz, L.,
- Jensen, N. R., Lamarque, J. F., Naik, V., Oltmans, S. J., Schwab, J., Shindell, D. T., Thompson, A. M., Thouret, V., Wang, Y., 12
- 13 and Zbinden, R. M.: Global distribution and trends of tropospheric ozone: An observation-based review, Elementa, 2,
- 14 https://doi.org/10.12952/journal.elementa.000029, 2014.
- 15 Cooper, O. R., Schultz, M. G., Schroeder, S., Chang, K.-L., Gaudel, A., Benítez, G. C., Cuevas, E., Fröhlich, M.,
- Galbally, I. E., Molloy, S., Kubistin, D., Lu, X., McClure-Begley, A., Nédélec, P., O'Brien, J., Oltmans, S. J., 16
- 17 Petropavlovskikh, I., Ries, L., Senik, I., Sjöberg, K., Solberg, S., Spain, G. T., Spangl, W., Steinbacher, M., Tarasick, D.,
- 18 Thouret, V., and Xu, X.: Multi-decadal surface ozone trends at globally distributed remote locations, Elementa: Science of the
- 19 Anthropocene, 8, 23, https://doi.org/10.1525/elementa.420, 2020.
- 20 Crutzen, P. J.: Tropospheric Ozone: An Overview, in: Tropospheric Ozone, Springer Netherlands, Dordrecht, 3–32, 21 https://doi.org/10.1007/978-94-009-2913-5 1, 1988.
- Crutzen, P. J., Lawrence, M. G., and Pöschl, U.: On the background photochemistry of tropospheric ozone, Tellus B: 22
- 23 Chemical and Physical Meteorology, 51, 123, https://doi.org/10.3402/tellusb.v51i1.16264, 1999.
- 24 Cui, J., Sprenger, M., Staehelin, J., Siegrist, A., Kunz, M., Henne, S., and Steinbacher, M.: Impact of stratospheric
- 25 intrusions and intercontinental transport on ozone at Jungfraujoch in 2005: Comparison and validation of two Lagrangian
- 26 approaches, Atmos Chem Phys, 9, 3371–3383, https://doi.org/10.5194/acp-9-3371-2009, 2009.
- 27 Daskalakis, N., Gallardo, L., Kanakidou, M., Nüß, J. R., Menares, C., Rondanelli, R., Thompson, A. M., and
- 28 Vrekoussis, M.: Impact of biomass burning and stratospheric intrusions in the remote South Pacific Ocean troposphere, Atmos
- 29 Chem Phys, 22, 4075–4099, https://doi.org/10.5194/acp-22-4075-2022, 2022.
- 30 East, J. D., Jacob, D. J., Balasus, N., Bloom, A. A., Bruhwiler, L., Chen, Z., Kaplan, J. O., Mickley, L. J., Mooring,
- 31 T. A., Penn, E., Poulter, B., Sulprizio, M. P., Worden, J. R., Yantosca, R. M., and Zhang, Z.: Interpreting the Seasonality of
- 32 Atmospheric Methane, Geophys Res Lett, 51, https://doi.org/10.1029/2024GL108494, 2024.
- 33 Fleming, Z. L., Doherty, R. M., Von Schneidemesser, E., Malley, C. S., Cooper, O. R., Pinto, J. P., Colette, A., Xu,
- 34 X., Simpson, D., Schultz, M. G., Lefohn, A. S., Hamad, S., Moolla, R., Solberg, S., and Feng, Z.: Tropospheric Ozone





- 1 Assessment Report: Present-day ozone distribution and trends relevant to human health, Elementa, 6, 12,
- 2 https://doi.org/10.1525/elementa.273, 2018.
- Forster, P., T. S. K. A. W. C. J.-L. D. D. F. D. J. L. T. M. M. D. P. M. W. M. W. and H. Z.: The Earth's Energy
- 4 Budget, Climate Feedbacks and Climate Sensitivity, in: Climate Change 2021 The Physical Science Basis, Cambridge
- 5 University Press, 923–1054, https://doi.org/10.1017/9781009157896.009, 2021.
- 6 Franzke, C.: Nonlinear trends, long-range dependence, and climate noise properties of surface temperature, J Clim,
- 7 25, 4172–4183, https://doi.org/10.1175/JCLI-D-11-00293.1, 2012.
- 8 Fu, B., Gasser, T., Li, B., Tao, S., Ciais, P., Piao, S., Balkanski, Y., Li, W., Yin, T., Han, L., Li, X., Han, Y., An, J.,
- 9 Peng, S., and Xu, J.: Short-lived climate forcers have long-term climate impacts via the carbon-climate feedback, Nat Clim
- 10 Chang, 10, 851–855, https://doi.org/10.1038/s41558-020-0841-x, 2020.
- Fuenzalida, H. A., Sánchez, R., and Garreaud, R. D.: A climatology of cutoff lows in the Southern Hemisphere,
- Journal of Geophysical Research D: Atmospheres, 110, 1–10, https://doi.org/10.1029/2005JD005934, 2005.
- Gallardo, L., Carrasco, J., and Olivares, G.: An analysis of ozone measurements at Cerro Tololo (30°S, 70°W, 2200
- 14 m.a.s.l.) in Chile, Tellus B Chem Phys Meteorol, 52, 50–59, https://doi.org/10.3402/tellusb.v52i1.16081, 2000.
- Gallardo, L., Henríquez, A., Thompson, A. M., Rondanelli, R., Carrasco, J., Orfanoz-Cheuquelaf, A., and Squez, P.
- 16 V.: The first twenty years (1994-2014) of ozone soundings from Rapa Nui (27°S, 109°W, 51m a.s.l.), Tellus B Chem Phys
- 17 Meteorol, 68, 29484, https://doi.org/10.3402/tellusb.v68.29484, 2016.
- 18 Garreaud, R. D., Vuille, M., Compagnucci, R., and Marengo, J.: Present-day South American climate, Palaeogeogr
- 19 Palaeoclimatol Palaeoccol, 281, 180–195, https://doi.org/10.1016/j.palaeo.2007.10.032, 2009.
- Garreaud, R. D., Boisier, J. P., Rondanelli, R., Montecinos, A., Sepúlveda, H. H., and Veloso-Aguila, D.: The Central
- 21 Chile Mega Drought (2010–2018): A climate dynamics perspective, International Journal of Climatology, 40, 421–439,
- 22 https://doi.org/10.1002/joc.6219, 2020.
- 23 Gaudel, A., Cooper, O. R., Ancellet, G., Barret, B., Boynard, A., Burrows, J. P., Clerbaux, C., Coheur, P.-F., Cuesta,
- 24 J., Cuevas, E., Doniki, S., Dufour, G., Ebojie, F., Foret, G., Garcia, O., Granados-Muñoz, M. J., Hannigan, J. W., Hase, F.,
- Hassler, B., Huang, G., Hurtmans, D., Jaffe, D., Jones, N., Kalabokas, P., Kerridge, B., Kulawik, S., Latter, B., Leblanc, T.,
- Le Flochmoën, E., Lin, W., Liu, J., Liu, X., Mahieu, E., McClure-Begley, A., Neu, J. L., Osman, M., Palm, M., Petetin, H.,
- Petropavlovskikh, I., Querel, R., Rahpoe, N., Rozanov, A., Schultz, M. G., Schwab, J., Siddans, R., Smale, D., Steinbacher,
- 28 M., Tanimoto, H., Tarasick, D. W., Thouret, V., Thompson, A. M., Trickl, T., Weatherhead, E., Wespes, C., Worden, H. M.,
- 29 Vigouroux, C., Xu, X., Zeng, G., and Ziemke, J.: Tropospheric Ozone Assessment Report: Present-day distribution and trends
- 30 of tropospheric ozone relevant to climate and global atmospheric chemistry model evaluation, Elementa: Science of the
- 31 Anthropocene, 6, https://doi.org/10.1525/elementa.291, 2018.
- 32 González, M. E., Gómez-González, S., Lara, A., Garreaud, R., and Díaz-Hormazábal, I.: The 2010–2015
- 33 Megadrought and its influence on the fire regime in central and south-central Chile, Ecosphere, 9,
- 34 https://doi.org/10.1002/ecs2.2300, 2018.





- 1 Griffiths, P. T., Murray, L. T., Zeng, G., Shin, Y. M., Abraham, N. L., Archibald, A. T., Deushi, M., Emmons, L. K.,
- 2 Galbally, I. E., Hassler, B., Horowitz, L. W., Keeble, J., Liu, J., Moeini, O., Naik, V., O'Connor, F. M., Oshima, N., Tarasick,
- 3 D., Tilmes, S., Turnock, S. T., Wild, O., Young, P. J., and Zanis, P.: Tropospheric ozone in CMIP6 simulations, Atmos Chem
- 4 Phys, 21, 4187–4218, https://doi.org/10.5194/acp-21-4187-2021, 2021.
- 5 Gulev, S.K., P.W. Thorne, J. Ahn, F.J. Dentener, C.M. Domingues, S. Gerland, D. Gong, D.S. Kaufman, H.C.
- 6 Nnamchi, J. Quaas, J.A. Rivera, S. Sathyendranath, S.L. Smith, B. Trewin, K. von Schuckmann, and R.S. Vose: Changing
- 7 State of the Climate System, in: Climate Change 2021 The Physical Science Basis, edited by: (IPCC), I. P. on C. C.,
- 8 Cambridge University Press, Cambridge, 287–422, https://doi.org/10.1017/9781009157896.004, 2023.
- 9 Hastie, T. and Tibshirani, R.: Generalized Additive Models, Statistical Science, 1, 10 https://doi.org/10.1214/ss/1177013604, 1986.
- Hastie, T., Tibshirani, R., and Friedman, J.: Boosting and Additive Trees, 1–51, https://doi.org/10.1007/b94608_10, 2009.
- He, J., Naik, V., Horowitz, L. W., Dlugokencky, E., and Thoning, K.: Investigation of the global methane budget over 1980–2017 using GFDL-AM4.1, Atmos Chem Phys, 20, 805–827, https://doi.org/10.5194/acp-20-805-2020, 2020.
- Hersbach, H., Bell, B., Berrisford, P., Hirahara, S., Horányi, A., Muñoz-Sabater, J., Nicolas, J., Peubey, C., Radu, R.,
- Schepers, D., Simmons, A., Soci, C., Abdalla, S., Abellan, X., Balsamo, G., Bechtold, P., Biavati, G., Bidlot, J., Bonavita, M.,
- 17 De Chiara, G., Dahlgren, P., Dee, D., Diamantakis, M., Dragani, R., Flemming, J., Forbes, R., Fuentes, M., Geer, A.,
- Haimberger, L., Healy, S., Hogan, R. J., Hólm, E., Janisková, M., Keeley, S., Laloyaux, P., Lopez, P., Lupu, C., Radnoti, G.,
- de Rosnay, P., Rozum, I., Vamborg, F., Villaume, S., and Thépaut, J.: The ERA5 global reanalysis, Quarterly Journal of the
- 20 Royal Meteorological Society, 146, 1999–2049, https://doi.org/10.1002/qj.3803, 2020.
- Hoesly, R. M., Smith, S. J., Feng, L., Klimont, Z., Janssens-Maenhout, G., Pitkanen, T., Seibert, J. J., Vu, L., Andres,
- 22 R. J., Bolt, R. M., Bond, T. C., Dawidowski, L., Kholod, N., Kurokawa, J. I., Li, M., Liu, L., Lu, Z., Moura, M. C. P., O'Rourke,
- 23 P. R., and Zhang, Q.: Historical (1750-2014) anthropogenic emissions of reactive gases and aerosols from the Community
- 24 Emissions Data System (CEDS), Geosci Model Dev, 11, 369–408, https://doi.org/10.5194/gmd-11-369-2018, 2018.
- Hu, Y., Huang, H., and Zhou, C.: Widening and weakening of the Hadley circulation under global warming, Sci Bull (Beijing), 63, 640–644, https://doi.org/10.1016/j.scib.2018.04.020, 2018.
- Jacob, D. J. and Winner, D. A.: Effect of climate change on air quality, Atmos Environ, 43, 51–63, https://doi.org/10.1016/j.atmosenv.2008.09.051, 2009.
- 29 Kalthoff, N., Bischoff-Gauß, I., Fiebig-Wittmaack, M., Fiedler, F., Thürauf, J., Novoa, E., Pizarro, C., Castillo, R.,
- 30 Gallardo, L., Rondanelli, R., and Kohler, M.: Mesoscale wind regimes in Chile at 30°S, Journal of Applied Meteorology, 41,
- 31 953–970, https://doi.org/10.1175/1520-0450(2002)041<0953:MWRICA>2.0.CO;2, 2002.
- Kovács, L.: Feature selection algorithms in generalized additive models under concurvity, Comput Stat, 39, 461–493,
- 33 https://doi.org/10.1007/s00180-022-01292-7, 2024.





- Kuai, L., Bowman, K. W., Worden, H. M., Herman, R. L., and Kulawik, S. S.: Hydrological controls on the tropospheric ozone greenhouse gas effect, Elementa: Science of the Anthropocene, 5, https://doi.org/10.1525/elementa.208, 2017.
- Kumar Mishra, A., Sen Gupta, G., Abha Singh, A., Bhushan Agrawal, S., and Tiwari, S.: Can fertilization OF CO2 heal the ozone-injured agroecosystems?, Atmos Pollut Res, 15, 102046, https://doi.org/10.1016/j.apr.2024.102046, 2024.
- Lapere, R., Mailler, S., and Menut, L.: The 2017 Mega-Fires in Central Chile: Impacts on Regional Atmospheric Composition and Meteorology Assessed from Satellite Data and Chemistry-Transport Modeling, Atmosphere (Basel), 12, 344, https://doi.org/10.3390/atmos12030344, 2021.
- 9 Li, Y., Xia, Y., Xie, F., and Yan, Y.: Influence of stratosphere-troposphere exchange on long-term trends of surface ozone in CMIP6, Atmos Res, 297, 107086, https://doi.org/10.1016/j.atmosres.2023.107086, 2024.
- Lipovetsky, S. and Conklin, M.: Analysis of regression in game theory approach, Appl Stoch Models Bus Ind, 17, 319–330, https://doi.org/10.1002/asmb.446, 2001.
- Lu, X., Zhang, L., Zhao, Y., Jacob, D. J., Hu, Y., Hu, L., Gao, M., Liu, X., Petropavlovskikh, I., McClure-Begley,
- 14 A., and Querel, R.: Surface and tropospheric ozone trends in the Southern Hemisphere since 1990: possible linkages to
- poleward expansion of the Hadley circulation, Sci Bull (Beijing), 64, 400–409, https://doi.org/10.1016/j.scib.2018.12.021,
- 17 Van Marle, M. J. E., Kloster, S., Magi, B. I., Marlon, J. R., Daniau, A. L., Field, R. D., Arneth, A., Forrest, M.,
- Hantson, S., Kehrwald, N. M., Knorr, W., Lasslop, G., Li, F., Mangeon, S., Yue, C., Kaiser, J. W., and Van Der Werf, G. R.:
- 19 Historic global biomass burning emissions for CMIP6 (BB4CMIP) based on merging satellite observations with proxies and
- 20 fire models (1750-2015), https://doi.org/10.5194/gmd-10-3329-2017, 11 September 2017.
- 21 Mills, G., Harmens, H., Wagg, S., Sharps, K., Hayes, F., Fowler, D., Sutton, M., and Davies, B.: Ozone impacts on
- 22 vegetation in a nitrogen enriched and changing climate, Environmental Pollution, 208, 898-908,
- 23 https://doi.org/10.1016/j.envpol.2015.09.038, 2016.
- Molnar, C.: Interpretable Machine Learning. A Guide for Making Black Box Models Explainable., Third Edition.,
- 25 247 pp., 2025.

2019.

- 26 Muggeo, V. M. R.: Interval estimation for the breakpoint in segmented regression: a smoothed score-based approach,
- 27 Aust N Z J Stat, 59, 311–322, https://doi.org/10.1111/anzs.12200, 2017.
- Murray, L. T., Mickley, L. J., Kaplan, J. O., Sofen, E. D., Pfeiffer, M., and Alexander, B.: Factors controlling
- variability in the oxidative capacity of the troposphere since the Last Glacial Maximum, Atmos Chem Phys, 14, 3589–3622,
- 30 https://doi.org/10.5194/acp-14-3589-2014, 2014.
- 31 Myhre, G., Shindell, D., Bréon, F.-M., Collins, W., Fuglestvedt, J., Huang, J., Koch, D., Lamarque, J.-F., Lee, D.,
- 32 Mendoza, B., Nakajima, T., Robock, A., Stephens, G., Takemura, T., and Zhang, H.: Anthropogenic and Natural Radiative
- 33 Forcing, in: Climate Change 2013: The Physical Science Basis. Contribution of Working Group I to the Fifth Assessment
- Report of the Intergovernmental Panel on Climate Change, edited by: Stocker, T. F., Qin, D., Plattner, G.-K., Tignor, M.,





- 1 Allen, S. K., Boschung, J., Nauels, A., Xia, Y., Bex, V., and Midgley, P. M., Cambridge University Press, 659–740,
- 2 https://doi.org/10.1017/CBO9781107415324.018, 2013.
- 3 Nisbet, E. G., Manning, M. R., Dlugokencky, E. J., Fisher, R. E., Lowry, D., Michel, S. E., Myhre, C. L., Platt, S. M.,
- 4 Allen, G., Bousquet, P., Brownlow, R., Cain, M., France, J. L., Hermansen, O., Hossaini, R., Jones, A. E., Levin, I., Manning,
- 5 A. C., Myhre, G., Pyle, J. A., Vaughn, B. H., Warwick, N. J., and White, J. W. C.: Very Strong Atmospheric Methane Growth
- 6 in the 4 Years 2014–2017: Implications for the Paris Agreement, Global Biogeochem Cycles, 33, 318–342,
- 7 https://doi.org/10.1029/2018GB006009, 2019.
- 8 Nuvolone, D., Petri, D., and Voller, F.: The effects of ozone on human health, Environmental Science and Pollution
- 9 Research, 25, 8074–8088, https://doi.org/10.1007/s11356-017-9239-3, 2018.
- Porter, W. C. and Heald, C. L.: The mechanisms and meteorological drivers of the summertime ozoneerature
- 11 relationship, Atmos Chem Phys, 19, 13367–13381, https://doi.org/10.5194/acp-19-13367-2019, 2019.
- Pusede, S. E., Steiner, A. L., and Cohen, R. C.: Temperature and Recent Trends in the Chemistry of Continental
- 13 Surface Ozone, https://doi.org/10.1021/cr5006815, 27 May 2015.
- Rondanelli, R.: Cutoff Lows Over Southwestern South America, in: Oxford Research Encyclopedia of Climate
- 15 Science, Oxford University Press, Oxford, https://doi.org/10.1093/acrefore/9780190228620.013.976, 2025.
- 16 Rondanelli, R., Gallardo, L., and Garreaud, R. D.: Rapid changes in ozone mixing ratios at Cerro Tololo (30°10'S,
- 17 70°48′W, 2200 m) in connection with cutoff lows and deep troughs, Journal of Geophysical Research Atmospheres, 107, ACL
- 18 6-1-ACL 6-15, https://doi.org/10.1029/2001JD001334, 2002.
- Rowlinson, M. J., Rap, A., Arnold, S. R., Pope, R. J., Chipperfield, M. P., McNorton, J., Forster, P., Gordon, H.,
- 20 Pringle, K. J., Feng, W., Kerridge, B. J., Latter, B. L., and Siddans, R.: Impact of El Niño-Southern Oscillation on the
- interannual variability of methane and tropospheric ozone, Atmos Chem Phys, 19, 8669–8686, https://doi.org/10.5194/acp-
- 22 19-8669-2019, 2019.
- 23 Saunois, M., Stavert, A. R., Poulter, B., Bousquet, P., Canadell, J. G., Jackson, R. B., Raymond, P. A., Dlugokencky,
- 24 E. J., Houweling, S., Patra, P. K., Ciais, P., Arora, V. K., Bastviken, D., Bergamaschi, P., Blake, D. R., Brailsford, G.,
- 25 Bruhwiler, L., Carlson, K. M., Carrol, M., Castaldi, S., Chandra, N., Crevoisier, C., Crill, P. M., Covey, K., Curry, C. L.,
- Etiope, G., Frankenberg, C., Gedney, N., Hegglin, M. I., Höglund-Isaksson, L., Hugelius, G., Ishizawa, M., Ito, A., Janssens-
- Maenhout, G., Jensen, K. M., Joos, F., Kleinen, T., Krummel, P. B., Langenfelds, R. L., Laruelle, G. G., Liu, L., Machida, T.,
- Maksyutov, S., McDonald, K. C., McNorton, J., Miller, P. A., Melton, J. R., Morino, I., Müller, J., Murguia-Flores, F., Naik,
- V., Niwa, Y., Noce, S., O'Doherty, S., Parker, R. J., Peng, C., Peng, S., Peters, G. P., Prigent, C., Prinn, R., Ramonet, M.,
- Regnier, P., Riley, W. J., Rosentreter, J. A., Segers, A., Simpson, I. J., Shi, H., Smith, S. J., Steele, L. P., Thornton, B. F., Tian,
- 31 H., Tohjima, Y., Tubiello, F. N., Tsuruta, A., Viovy, N., Voulgarakis, A., Weber, T. S., van Weele, M., van der Werf, G. R.,
- Weiss, R. F., Worthy, D., Wunch, D., Yin, Y., Yoshida, Y., Zhang, W., Zhang, Z., Zhao, Y., Zheng, B., Zhu, Q., Zhu, Q., and
- 33 Zhuang, Q.: The Global Methane Budget 2000–2017, Earth Syst Sci Data, 12, 1561–1623, https://doi.org/10.5194/essd-12-
- 34 1561-2020, 2020.





- 1 Schwertfeger, B. T., Lohmann, G., and Lipskoch, H.: Introduction of the BiasAdjustCXX command-line tool for the 2 of application fast and efficient bias corrections in climatic research. SoftwareX, 22, 3 https://doi.org/10.1016/j.softx.2023.101379, 2023.
- Seguel, R. J., Morales S., R. G. E., and Leiva G., M. A.: Ozone weekend effect in Santiago, Chile, Environmental Pollution, 162, 72–79, https://doi.org/10.1016/j.envpol.2011.10.019, 2012.
- 6 Seguel, R. J., Castillo, L., Opazo, C., Rojas, N. Y., Nogueira, T., Cazorla, M., Gavidia-Calderón, M., Gallardo, L.,
- 7 Garreaud, R., Carrasco-Escaff, T., and Elshorbany, Y.: Changes in South American surface ozone trends: exploring the
- 8 influences of precursors and extreme events, Atmos Chem Phys, 24, 8225–8242, https://doi.org/10.5194/acp-24-8225-2024,
- 9 2024.
- Sekiya, T. and Sudo, K.: Role of meteorological variability in global tropospheric ozone during 1970–2008, Journal of Geophysical Research: Atmospheres, 117, https://doi.org/10.1029/2012JD018054, 2012.
- 12 Skeie, R. B., Myhre, G., Hodnebrog, Ø., Cameron-Smith, P. J., Deushi, M., Hegglin, M. I., Horowitz, L. W., Kramer,
- 13 R. J., Michou, M., Mills, M. J., Olivié, D. J. L., Connor, F. M. O., Paynter, D., Samset, B. H., Sellar, A., Shindell, D., Takemura,
- 14 T., Tilmes, S., and Wu, T.: Historical total ozone radiative forcing derived from CMIP6 simulations, NPJ Clim Atmos Sci, 3,
- 15 https://doi.org/10.1038/s41612-020-00131-0, 2020.
- Škerlak, B., Sprenger, M., and Wernli, H.: A global climatology of stratosphere-troposphere exchange using the ERA-Interim data set from 1979 to 2011, Atmos Chem Phys, 14, 913–937, https://doi.org/10.5194/acp-14-913-2014, 2014.
- Snyder, C. W., Mastrandrea, M. D., and Schneider, S. H.: The Complex Dyanmics of the Climate System: Constraints on our Knowledge, Policy Implications and the Necessity of Systems Thinking, in: Philosophy of complex systems, Elsevier,
- 20 467–505, 2011.
- Staehle, C., Rieder, H. E., Fiore, A. M., and Schnell, J. L.: Technical note: An assessment of the performance of statistical bias correction techniques for global chemistry–climate model surface ozone fields, Atmos Chem Phys, 24, 5953–
- 23 5969, https://doi.org/10.5194/acp-24-5953-2024, 2024.
- 24 Szopa, S., V. N. B. A. P. A. T. B. W. D. C. S. F. L. G. A. K.-S. Z. K. H. L. N. U. and P. Z.: Short-lived Climate
- 25 Forcers, in: Climate Change 2021 The Physical Science Basis, edited by: Masson-Delmotte, V., P. Zhai, A. Pirani, S.L.
- 26 Connors, C. Péan, S. Berger, N. Caud, Y. Chen, L. Goldfarb, M. I. G. and M. Huang, K. Leitzell, E. Lonnoy, J.B.R. Matthews,
- 27 T.K. Maycock, T. Waterfield, O. Yelekçi, R. Yu, and B. Z., Cambridge University Press, United Kingdom and New York,
- 28 NY, USA, 817–922, https://doi.org/10.1017/9781009157896.008, 2021.
- Thompson, A. M.: The oxidizing capacity of the Earth's atmosphere: Probable past and future changes, Science
- 30 (1979), 256, 1157–1165, https://doi.org/10.1126/science.256.5060.1157, 1992.
- Thoning, K. W., Tans, P. P., and Komhyr, W. D.: Atmospheric carbon dioxide at Mauna Loa Observatory: 2. Analysis
- 32 of the NOAA GMCC data, 1974-1985, Journal of Geophysical Research: Atmospheres, 94, 8549-8565,
- 33 https://doi.org/10.1029/JD094iD06p08549, 1989.





- 1 Wang, S., Foster, A., Lenz, E. A., Kessler, J. D., Stroeve, J. C., Anderson, L. O., Turetsky, M., Betts, R., Zou, S., and
- 2 Liu, W.: Mechanisms and impacts of Earth system tipping elements, Reviews of Geophysics, 61, e2021RG000757, 2023.
- Weatherhead, E. C., Reinsel, G. C., Tiao, G. C., Meng, X. L., Choi, D., Cheang, W. K., Keller, T., DeLuisi, J.,
- 4 Wuebbles, D. J., Kerr, J. B., Miller, A. J., Oltmans, S. J., and Frederick, J. E.: Factors affecting the detection of trends:
- 5 Statistical considerations and applications to environmental data, Journal of Geophysical Research Atmospheres, 103, 17149–
- 6 17161, https://doi.org/10.1029/98JD00995, 1998.
- Weber, T., Wiseman, N. A., and Kock, A.: Global ocean methane emissions dominated by shallow coastal waters,
- 8 Nat Commun, 10, 4584, https://doi.org/10.1038/s41467-019-12541-7, 2019.
- 9 Yeung, L. Y., Murray, Lee. T., Martinerie, P., Witrant, E., Hu, H., Banerjee, A., Orsi, A., and Chappellaz, J.: Isotopic
- 10 constraint on the twentieth-century increase in tropospheric ozone, Nature, 570, 224–227, https://doi.org/10.1038/s41586-019-
- 11 1277-1, 2019.
- 12 Young, P. J., Archibald, A. T., Bowman, K. W., Lamarque, J.-F., Naik, V., Stevenson, D. S., Tilmes, S., Voulgarakis,
- 13 A., Wild, O., Bergmann, D., Cameron-Smith, P., Cionni, I., Collins, W. J., Dalsøren, S. B., Doherty, R. M., Eyring, V.,
- 14 Faluvegi, G., Horowitz, L. W., Josse, B., Lee, Y. H., MacKenzie, I. A., Nagashima, T., Plummer, D. A., Righi, M., Rumbold,
- 15 S. T., Skeie, R. B., Shindell, D. T., Strode, S. A., Sudo, K., Szopa, S., and Zeng, G.: Pre-industrial to end 21st century
- 16 projections of tropospheric ozone from the Atmospheric Chemistry and Climate Model Intercomparison Project (ACCMIP),
- 17 Atmos Chem Phys, 13, 2063–2090, https://doi.org/10.5194/acp-13-2063-2013, 2013.
- Zhang, Y., Cooper, O. R., Gaudel, A., Thompson, A. M., Nédélec, P., Ogino, S. Y., and West, J. J.: Tropospheric
- 19 ozone change from 1980 to 2010 dominated by equatorward redistribution of emissions, Nat Geosci, 9, 875–879,
- 20 https://doi.org/10.1038/ngeo2827, 2016.
- 21 Zhang, Y., West, J. J., Emmons, L. K., Flemming, J., Jonson, J. E., Lund, M. T., Sekiya, T., Sudo, K., Gaudel, A.,
- 22 Chang, K., Nédélec, P., and Thouret, V.: Contributions of World Regions to the Global Tropospheric Ozone Burden Change
- 23 From 1980 to 2010, Geophys Res Lett, 48, https://doi.org/10.1029/2020GL089184, 2021.